UNCLASSIFIED

(2)

AD-A158 390

DTIC FILE COPY

SECURITY CLASSIFICATION OF THIS PAGE (When Data Entered)

REPORT DOCUMENTATION PAGE	READ INSTRUCTIONS BEFORE COMPLETING FORM
1. REPORT NUMBER: AFOSR-TR- 85-0581	2. GOVT ACCESSION NO. / 3. RECIPIENT'S CATALOG NUMBER
4. TITLE (and Subtitle): Lg Wave Excitation and Propagation with Application to Nuclear Yield Determination	5. TYPE OF REPORT & PERIOD COVERED: Final Report 4/1/83 - 3/31/85
	6. PERFORMING ORG. REPORT NUMBER
7. AUTHOR(s): Robert B. Herrmann, Chien-Ying Wang	8. CONTRACT OR GRANT NUMBER(s): F49620-83-C-0087
9. PERFORMING ORGANIZATION NAME AND ADDRESS: Dept. of Earth & Atmospheric Sciences, Saint Louis University, St. Louis, MO 63156	10. PROGRAM ELEMENT, PROJECT, TASK AREA & WORK UNIT NUMBERS: ARPA Order 4751, Program Code 3D60
11. CONTROLLING OFFICE NAME AND ADDRESS: DARPA, 1400 Wilson Blvd., Arlington, VA 27709	12. REPORT DATE: 28 May 1985
	13. NUMBER OF PAGES: 72 + 3
14. MONITORING AGENCY NAME & ADDRESS(if different from Controlling Office): AFOSR, Bolling AFB, DC 20332	15. SECURITY CLASS. (of this report): Unclassified
	15a. DECLASSIFICATION DOWNGRADING SCHEDULE

16. DISTRIBUTION STATEMENT (of this Report)

Approved for public release. Distribution unlimited.

17. DISTRIBUTION STATEMENT (of the abstract entered in Block 20, if different from Report)

DTIC ELECTE AUG 23 1985 S D

18. SUPPLEMENTARY NOTES

19. KEY WORDS (Continue on reverse side if necessary and identify by block number)

Lg coda; Coda Q; Seismic Wave Scattering; Synthetic Seismograms

20. ABSTRACT (Continue on reverse side if necessary and identify by block number)

Malin's (1980) first-order single scattering theory has been extended to study the scattering of surface waves as well as body waves by distributed point scatterers in a layered medium. The scattered waveform itself is generated and examined instead of its energy envelope. The theory used allows; 1) mode conversion; 2) wave type conversion; 3) finite scatterer distribution; and 4) the effect of attenuation from scattering as well as intrinsic

(continued)

DD FORM 1 JAN 73 1473

UNCLASSIFIED

20. Abstract (continued)

absorption. The cases studied are for elastic or slightly attenuative media with any kind of source and receiver at any place in the layered structure. This direct calculation of coda waves provides us an immediate description of the relation of coda and scattering. The objectives are to find 1) the effect of layering on scattering; 2) the effect of scatterer distribution on recorded vertical and horizontal motion; 3) the relation of scattering Q to intrinsic Q; 4) the scattering behavior of surface and body waves; and 5) the superposition of scattering waves to form the coda. The generation of body waves by 'locked mode' approximation, which makes the body wave a subset of the 'surface wave,' is extensively studied. The preliminary results explain some observed coda behaviors surprisingly well. We find a larger geometrical spreading for near scatterers, which is caused by mode conversion or wavetype conversion because of the wide angle scattering. This makes the spreading correction higher for the early part of the coda which may compensate the low Q observed in the early coda of regional earthquakes. This study is of practical value as an effort to understand the complicated coda phases.

Final Technical Report

1 April 1983 - 31 March 1985

ARPA Order No.:	4751
Program Code:	5H133
Contractor:	Saint Louis University
Effective Date of Contract:	1 April 1983
Contract Expiration Date:	31 March 1985
Amount of Contract:	$141,624.00
Contract Number:	F49620-83-C-0087
Principal Investigators:	Robert B. Herrmann (314-658-3120) Chien-Ying Wang (314-658-3197)
Short Title:	Lg Wave Excitation

Spondored by

Advanced Research Projects Agency (DOD)

ARPA Order No. 4751

Monitored by AFOSR under Contract #F49620-83-C-0087

Table of Contents

Technical Report Summary

Malin's (1980) first-order single scattering theory has been extended to study the scattering of surface waves as well as body waves by distributed point scatterers in a layered medium. The scattered waveform itself is generated and examined instead of its energy envelope. The theory used allows 1) mode conversion 2) wave type conversion 3) finite scatterer distribution, and 4) the effect of attenuation from scattering as well as intrinsic absorption. The cases studied are for elastic or slightly attenuative media with any kind of source and receiver at any place in the layered structure. This direct calculation of coda waves provides us an immediate description of the relation of coda and scattering. The objectives are to find 1) the effect of layering on scattering, 2) the effect of scatterer distribution on recorded vertical and horizontal motion, 3) the relation of scattering Q to intrinsic Q, 4) the scattering behavior of surface and body waves, and 5) the superposition of scattering waves to form the coda. The generation of body waves by 'locked mode' approximation, which makes the body wave a subset of the 'surface wave', is extensively studied. The prelimilary results explain some observed coda behaviors surprisingly well. We find a larger geometrical spreading for near scatterers, which is caused by mode conversion or wavetype conversion because of the wide angle scattering. This makes the spreading correction higher for early part of coda which may compensate the low Q observed in early coda of regional earthquakes. This study is of practical value as an effort to understand the complicated coda phases.

Synthesis of Coda Waves in the Layered Medium

Chien-Ying Wang and Robert B. Herrmann

Introduction

Because of recent interest on attempting to extract useful information from the coda, a theoretical study of coda waves is urgently required, especially since the theory lags behind observations. Most of current coda analyses are based on Aki's (1969) backscattering model, which was extended by Herrmann (1980) to determine coda Q. This model treats the coda as a smoothly decaying envelope which is formed by many randomly scattered waves. Figure 1a is a real seismogram from the ECTN network. The envelope has an exponential decaying form. Taking a closer look, however, the decay is not so uniform. Figure 1b shows the rectified signal. The seismogram looks as if it is composed of many small 'pulses' or 'beats'. This is even more obvious after bandpass filtering at 1 Hz (Figure 1c). It is interesting to see if such pulses can be analyzed separately.

Since the scattered wave is the result of an averaging process for waves reacting with randomly distributed scatterers, most theories take a stochastic approach and describe the total wavefield by several statistical quantities. Mean power spectral density is frequently used, for instance (Aki, 1969; Sato, 1977). Using such an approach, the analysis of data provides a gross description of the distributed inhomogeneities and the scattering process, but some ambiguities arise. The problem of distinguish between scattering Q and intrinsic Q is a typical example (Aki, 1982; Dainty, 1984). For our study, we choose a deterministic approach to investigate the effect of scattering on the generation of coda. We will directly examine each individual scattered pulse generated in the layered medium.

Sato (1984) proposed a scattering model which describes the body wave scattering due to a plane wave incident on the scatterers. A similar model is also found in Wu

and Aki (1985). This model considers the wave type conversion, scattering pattern, scatterer size, etc., but only for body waves in a homogeneous whole space. From another view point, Malin (1980) constructed a scattering model using surface wave normal mode theory. An important feature of this model is that it is able to handle multi-layered medium. The rays scattered by the inhomogeneities in a layered structure, such as the earth's crust, are numerous. It is only by using mode theory that scattering in such a medium can be treated.

In this study, we extend Malin's first-order single scattering model to create the scattering 'pulse' from scatterers situated in the layered structure. A simple review of this method is provided with the derivation largely simplified. In order to include the body wave scattering, we also discuss the 'locked mode' approximation (Harvey, 1981), which makes the body wave a subset of the surface-wave contribution. Each individual scattered wave is examined in detail rather than its statistical average. The study is directed toward understanding the nature of the scattered waves under different conditions. This enables us to analyze the behavior of each scatterer, and hence makes it easier to isolate important factors which may be lost in an averaging process.

First-Order Single Scattering Theory

The model considered is a layered medium (Figure 2) with inhomogeneities distributed at some restricted regions in it. The inhomogeneous region is assumed to be small compared to the wavelength. We call it a scatterer parcel. If the parcel is not small enough to be thought of as a point, we can divide it into several small parts and perform an integration to find the total field. For this study we just consider the point scatterer. This point scatterer generates secondary waves when acted upon by the incident wave. The scattered wave has the form of pulse with limited duration (Figure 3). The coda is thought to be composed of numerous such scattering pulses.

To satisfy the Born approximation (weak, single scattering), the inhomogeneities are assumed to be small perturbations of the background material:

$$\rho = \rho_0 + \delta\rho$$
$$C_{ijkl} = C_{0\,ijkl} + \delta C_{ijkl}$$

ρ is the density and C_{ijkl} is the elastic constant. For the isotropic elastic medium considered here, C_{ijkl}'s recuce to the Lame's constant λ or the rigidity μ . Since we just discuss the scattering from a small parcel, the mean behavior of these inhomogeneities is not assumed. These three parameters ρ, λ, and μ can be reduced to a single parameter, if there exist relations among them. Sato (1984) used the velocity perturbation;

$$\frac{\delta\alpha}{\alpha} = \frac{\delta\beta}{\beta} = \xi$$

and adopted Birch's law relating the density and wave velocity

$$\alpha = a_1 \rho + a_0 \qquad \beta = b_1 \rho + b_0$$

(a's and b's are constant). This results in

$$\frac{\delta\rho}{\rho} = v\,\xi \qquad \frac{\delta\lambda}{\lambda} = \frac{\delta\mu}{\mu} = (2 + v)\,\xi$$

The value of v is kept at 0.8 in this report. ξ will be the only parameter needed to describe the inhomogeneity variation under these assumptions. Wu (1984) used different values for density perturbation and elastic constant perturbation which results in two different types of inhomogeneities; impedance type and velocity type, each of which has different scattering properties. To reduce the number of independent parameters, we just use one parameter ξ to represent them.

As indicated by Hudson (1977), the scattered field for any first-order scattering theory can always be expressed using the representation theorem:

$$u_J^{(s)} = \int dV \left\{ \delta\rho\,\omega^2\,G_i^J\,u_i^0 - \delta C_{ijkl}\,\partial_j G_i^J\,\partial_l u_k^0 \right\}$$

For the isotropic elastic case, this is equivalent to

$$u_j^{(s)} = \int dV \left\{ \delta\rho\, \omega^2\, G_i^J\, u_i^0 - \delta\lambda\, \partial_i G_i^J\, \partial_j u_j^0 - \delta\mu\, \partial_j G_i^J\, (\partial_j u_i^0 + \partial_i u_j^0) \right\} \qquad (1)$$

where u_i^0 is the wave field incident on the inhomogeneous body, and G_i^J is the Green's function for the corresponding boundary conditions. For the case of body wave in a homogeneous space, G_i^J has the form as given by equation (4.30) in Aki and Richards (1980), which is used by Sato (1984) and Wu and Aki (1985). For the case of a surface wave in the layered medium, G_i^J can be determined by the normal mode theory (Malin, 1978).

The surface wave case is easier to construct since the incident wave and the scattered wave are trapped in the layers and propagate two dimensionally. From the surface wave mode theory (Wang, 1981), the incident wave field, which has the mode order m and wave type ν (ν =R for Rayleigh wave and L for Love wave), has the form

$$ {}^{\nu}u_m^0 = \frac{1}{\sqrt{2\pi\, {}^{\nu}k_m x}}\, {}^{\nu}s_m\, {}^{\nu}a_m\, e^{-i\, {}^{\nu}k_m x + i\frac{\pi}{4}}\, {}^{\nu}U_m \qquad (2)$$

$$ {}^{\nu}a_m = \frac{1}{2\, {}^{\nu}c_m\, {}^{\nu}g_m\, {}^{\nu}I_{0m}} $$

$$ {}^{R}U = \left[U_r\, ,\, 0\, ,\, -iU_z \right]_{\text{at scatterer}} $$

$$ {}^{L}U = \left[0\, ,\, U_\theta\, ,\, 0 \right]_{\text{at scatterer}} $$

where

k = wave number,

x = the distance between the source and the scatterer,

a = amplitude factor,

c = phase velocity,

g = group velocity,

I_0 = energy integral of surface waves.

U_r, U_z, U_θ = displacement eigenfunctions at the radial,

vertical and tangential direction,

The source term s_m for double-couple and explosive sources is given in the Appendix I. The Green's function with mode n and wave type η for the wave field after scattering is

$$ {}^{\eta}G_n^J = \frac{1}{\sqrt{2\pi\ {}^{\eta}k_n r}}\ {}^{\eta}U_n\ {}^{\eta}a_n\ e^{-i\,{}^{\eta}k_n r + i\frac{\pi}{4}}\ {}^{\eta}R_n^J \qquad (3) $$

$$ {}^{R}U = \left[U_r\cos\theta\ ,\ U_r\sin\theta\ ,\ -iU_z \right]_{\text{at scatterer}} $$

$$ {}^{R}R = \left[U_r\cos\phi\ ,\ U_r\sin\phi\ ,\ -iU_z \right]_{\text{at receiver}} $$

$$ {}^{L}U = \left[U_\phi\sin\theta\ ,\ -U_\phi\cos\theta\ ,\ 0 \right]_{\text{at scatterer}} $$

$$ {}^{L}R = \left[U_\phi\sin\phi\ ,\ -U_\phi\cos\phi\ ,\ 0 \right]_{\text{at receiver}} $$

r is the distance from the scatterer to the receiver. The scattering angle θ and the receiving angle ϕ are defined in Figure 2a. These angles are important since they control the recorded wavefield. Scattered P-SV waves can appear on the receiver horizontal component defined as tangential with respect to the source.

Substituting these functions into the equation (1), the scattered wave field ${}^{\nu\eta}u_{mn}$ which includes the conversion from mode m of wave type ν to mode n of wave type η, is written as

$$ {}^{\nu\eta}u_{mn}^{(s)} = \int dV \frac{1}{2\pi\sqrt{{}^{\nu}k_m x\ {}^{\eta}k_n r}}\ {}^{\nu}a_m\ {}^{\eta}a_n s_m R_n e^{-i({}^{\nu}k_m x + {}^{\eta}k_n r) + i\frac{\pi}{2}} $$
$$ \cdot(\delta\rho\omega^2\ {}^{\nu\eta}A_{mn} - \delta\lambda\ {}^{\nu\eta}B_{mn} - \delta\mu\ {}^{\nu\eta}C_{mn}) \qquad (4) $$

where

$$ {}^{RR}A_{mn} = U_{rm}\,U_{rn}\cos\theta + U_{zm}\,U_{zn} $$
$$ {}^{RR}B_{mn} = ({}^{R}k_m\,{}^{R}U_{rm} - \partial_z U_{zm})\,({}^{R}k_n\,U_{rn} - \partial_z U_{zn}) $$
$$ {}^{RR}C_{mn} = 2\,({}^{R}k_m U_{rm}\,{}^{R}k_n U_{rn}\cos^2\theta + \partial_z U_{zm}\partial_z U_{zn}) $$
$$ + ({}^{R}k_m U_{zm} + \partial_z U_{rm})\,({}^{R}k_n U_{zn} + \partial_z U_{rn})\cos\theta $$

$$ {}^{RL}A_{mn} = -U_{rm}\,U_{\theta n}\sin\theta $$
$$ {}^{RL}C_{mn} = -\,{}^{R}k_m U_{rm}\,{}^{L}k_n U_{\theta n}\sin 2\theta $$
$$ -\partial_z U_{\theta n}\,(\partial_z U_{rm} + {}^{R}k_m U_{zm})\sin\theta $$

$$ {}^{LR}A_{mn} = U_{\theta m}\,U_{rn}\sin\theta $$

$$
\begin{aligned}
{}^{LR}C_{mn} &= {}^{L}k_m U_{\phi m}\, {}^{R}k_n U_{rn} \sin 2\theta \\
&\quad + \partial_z U_{\phi m}\,(\partial_z U_{rn} + {}^{R}k_n U_{zn}) \sin\theta
\end{aligned}
$$

$$
{}^{LL}A_{mn} = U_{\phi m}\, U_{\phi n} \cos\theta
$$

$$
{}^{LL}C_{mn} = {}^{L}k_m U_{\phi m}\, {}^{L}k_n U_{\phi n} \cos 2\theta + \partial_z U_{\phi m}\, \partial_z U_{\phi n} \cos\theta
$$

We also define a scattering term F_{mn} as

$$
\begin{aligned}
{}^{\nu\eta}F_{mn} &= \int dV \left\{ e^{-i({}^{\nu}k_m x + {}^{\eta}k_n r) + i\frac{\pi}{2}} (\delta\rho\omega^2\, {}^{\nu\eta}A_{mn} - \delta\lambda\, {}^{\nu\eta}B_{mn} - \delta\mu\, {}^{\nu\eta}C_{mn}) \right\} \qquad (5) \\
&= \int dV \left\{ e^{-i({}^{\nu}k_m x + {}^{\eta}k_n r) + i\frac{\pi}{2}} \xi \left[v\rho\omega^2\, {}^{\nu\eta}A_{mn} - (2+v)\lambda\, {}^{\nu\eta}B_{mn} - (2+v)\mu\, {}^{\nu\eta}C_{mn} \right] \right\} \\
&= \int dV \left\{ e^{-i({}^{\nu}k_m x + {}^{\eta}k_n r) + i\frac{\pi}{2}} \xi\, {}^{\nu\eta}D_{mn} \right\}
\end{aligned}
$$

The final total field solution is the sum over all modes and conversions for all scatterers in the region. The scattering term F corresponds to the 'volume factor' of Wu and Aki (1985) if the Green's function related term D is not included. For a point scatterer, we simply use

$$
{}^{\nu\eta}F_{mn} = \delta V\, e^{-i({}^{\nu}k_m x + {}^{\eta}k_n r) + i\frac{\pi}{2}} \xi\, {}^{\nu\eta}D_{mn}
$$

with δV having the dimension of unit volume.

Scattering Q

To include the effect of energy loss due to scattering, Malin (1978) considered a correction which consevers energy to the first order by choosing a specific correlation function for the scattering cross section. Although we are interested in the behavior of each individual point scatterer, the scattering coefficient, or equivalently the cross section, is still needed when defining the scattering Q.

Let us consider a small scatterer parcel containing distributed inhomogeneities. For a single point scatterer, we can use a deterministic scattering formula. However, when a wave is incident on this scatterer parcel, the size of the scatterers within it, the

relative distance between individual point scatterers, and the wavelength of the incident wave will determine the partition of energy being scattered. From scattering theory, the parameter describing this property is the 'cross section' (Ishimaru, 1977, p.10). Within a unit of the scattering angle, the differential cross section σ_d is defined by

$$\sigma_d = \lim_{r\to\infty} \frac{r\ (\text{ scattered energy flux density})}{(\text{ incident energy flux density})} \tag{6}$$

The total scattering cross section is obtained by integration over all angles:

$$\sigma_s = \int_{2\pi} \sigma_d \, d\theta$$

When scatterers are distributed with the mean density n (particles per unit area at a constant depth for a two dimensional case), the scattering coefficient α which characterizes the intensity of the scattered wave excitation is given by

$$\alpha = n\,\sigma_s$$

The reciprocal of α is usually called the mean free path. Scattering coefficient α thus defined is equivalent to the turbidity in the two dimensional case as compared to Aki and Chouet (1976).

To obtain the energy flux density, the wave field excited in the layered medium should be taken into account:

$$<|u|^2> = \omega^2 \int dz \rho_0 <uu^*>$$

$<>$ means the average over the ensemble. Using equations (2) and (4), it is not difficult to find the scattering coefficient for mode pairs mn, and types $\nu\eta$ by setting r in equation (6) as the distance between the scatterer and the receiver:

$$\begin{aligned}
{}^{\nu\eta}\alpha_{mn} &= n \int_{2\pi} d\theta \frac{r <|{}^{\nu\eta}u_{mn}^{(s)}|^2>}{<|{}^{\nu}u_m^0|^2>} \\
&= \frac{1}{2\pi} \frac{{}^{\eta}a_n^{\,2}}{{}^{\eta}k_n} \frac{{}^{\eta}I_{0n}}{{}^{\nu}I_{0m}} \int_{2\pi} n <{}^{\nu\eta}F_{mn}^2> d\theta \\
&= \frac{1}{2\pi} \frac{{}^{\eta}a_n\ {}^{\nu}a_m\ {}^{\nu}g_m}{{}^{\nu}k_m\ {}^{\eta}g_n} \int_{2\pi} n <{}^{\nu\eta}F_{mn}^2> d\theta
\end{aligned}$$

$$= \frac{1}{2\pi} \, {}^{\eta\nu}A_{ma} \int_{2\pi} n < {}^{\nu\eta}F_{ma}^2 > d\theta$$

Now we have the problem of defining the average behavior of the function $< {}^{\nu\eta}F_{ma}^2 >$. Taking a closer look at the scattering region (Figure 2b), the scatterers are distributed over a plane area and the phase term in F_{ma}^2 (equation 5) is actually

$$\begin{aligned} e^{-i\vec{k}_m'\vec{x}' - i\vec{k}_n'\vec{r}'} &= e^{-ik_m(x+\vec{e}_x\vec{\varsigma}) - ik_n(r-\vec{e}_r\vec{\varsigma})} \\ &= e^{-ik_m x - ik_n r} \, e^{-i\vec{\varsigma}(k_m\vec{e}_x - k_n\vec{e}_r)} \\ &= e^{-ik_m x - ik_n r} \, e^{i\vec{\varsigma}\vec{k}_B} \end{aligned}$$

$\vec{k}_B = \vec{k}_n - \vec{k}_m$ is called the Bragg vector. Hence, in evaluating F_{ma} from equation (5),

$$\begin{aligned} F_{ma} &= \int dV \left\{ e^{-ik_m x - ik_n r + i\frac{\pi}{2}} \left[\xi(\vec{\varsigma}, z) \, e^{i\vec{\varsigma}\vec{k}_B} \right] D_{ma}(z) \right\} \\ &= \int dz \left\{ e^{-ik_m x - ik_n r + i\frac{\pi}{2}} \; \hat{\xi}\,(k_B, z) \, D_{ma}(z) \right\} \end{aligned}$$

where we have made a two dimensional Fourier transform for the scatterer distribution spectra in the horizontal direction (Kennett, 1972). The ensemble average of F_{ma} is thus

$$< F_{ma}^2 > = \int dz dz' \left\{ < \hat{\xi}(k_B, z) \; \hat{\xi}(k_B, z') > \; D_{ma}(z) \, D_{ma}(z') \right\}$$

$< \hat{\xi}\hat{\xi}' >$, the correlation function of inhomogeneity distribution, is usually given by a form of an exponential function or a Gaussian function (Chernov, 1960). Assuming that this function has a small side lobe, i.e., small correlation distance in the exponential form, we have a simpler form:

$$n < F_{ma}^2 > = \left[n \int dz dz' < \hat{\xi}(k_B, z) \; \hat{\xi}(k_B, z') > \right] D_{ma}^2(z) = U_{ss} \, D_{ma}^2(z)$$

The term in the bracket, which describes the condition of scatterer distribution around the point considered, will be kept together and called a scattering attenuation unit (U_{ss}) . U_{ss} is in the unit of km^4. If U_{ss} is maintained as a single value in the calculations,

this is equivalent to stating that the scattering environment is similar for all waves propagating in the layered medium. The expression above is perhaps too simplified. The correlation function must be specified if an accurate scattering cross section is desired. In this study, we just use the simplest form to examine its possible effect.

The scattering coefficient thus has the from:

$$
\begin{aligned}
{}^{RR}\alpha &= {}^{RR}A\, U_{sn} \left[\frac{3}{8}\, {}^{RR}\Theta_4 + \frac{1}{2}\, {}^{RR}\Theta_2 + {}^{RR}\Theta_0 \right] \\
{}^{RL}\alpha &= {}^{RL}A\, U_{sn} \left[\frac{1}{2}\, {}^{RL}\Theta_4 + \frac{1}{2}\, {}^{RL}\Theta_2 \right] \\
{}^{LR}\alpha &= {}^{LR}A\, U_{sn} \left[\frac{1}{2}\, {}^{LR}\Theta_4 + \frac{1}{2}\, {}^{LR}\Theta_2 \right] \\
{}^{LL}\alpha &= {}^{LL}A\, U_{sn} \left[\frac{1}{2}\, {}^{LL}\Theta_4 + \frac{1}{2}\, {}^{LL}\Theta_2 \right]
\end{aligned}
\qquad (7)
$$

Θ's are given in the Appendix I. We have used the distance r between the scatterer and the receiver to define the scattering coefficient (equation 6) and to calculate the incident energy flux and the scattered energy flux by fixing on the source-scatterer-receiver geometry. The mode pair mn reduces its energy by $e^{-\alpha_{mn}(r+x)}$ after trveling the distance from source to scatterer to receiver. The effect thus caused by the scattering of inhomgeneities is called the scattering attenuation.

Numerical Experiment I: Mode-conversion and Scatterer location

With the velocity model chosen (CUS model, see Table 1), we generate the eigenfunctions of surface waves, mainly the Lg wave, up to 5 Hz. Using these, the scattered waves are created by specifying the source (depth, mechanism), the receiver (distance, instrument), the scatterers (location, material variation, and scattering intensity), and the attenuation condition (intrinsic Q and scattering Q). To make the problem easier to follow, we fix the following, except as indicated otherwise:

source depth = 10 km

scatterer depth = 5 km

source time function = parabolic with base 0.4 second.

receiver distance = 100 km

waveform received = ground velocity

inhomogeneity variation = 5%

mode conversion = up to 10 neighboring modes (due to computer restriction on speed and storage)

wave type conversion = yes

An arbitrary source mechanism was used and the effect of its radiation pattern is averaged out by distributing several scatterers on the ellipse. In this section, we will discuss the properties of the scattered waves under different scattering conditions but ignore the problem of scattering and intrinsic attenuation at this moment. The so called 'diagonal selection' rule (Malin, 1980) which states that a particular mode of surface wave mainly scatters into the same mode without significant conversion will be examined first. Sscattering from different locations, e.g., distances, depths, scattering angle, etc., are also discussed.

Malin (1980) used scattering coefficient of vertical component from an acoustic model to justify the diagonal selection rule. Since the scattered wave instead of its energy envelope is generated here, this rule will be discussed by examining the resultant waveforms. Two cases are studied; one is for the wave type conversion (from R to L and L to R), and the other for the mode conversion. Figure 3 shows the waveforms of signals directly from the source (surface wave) or from a scatterer (scattered waves) after traveling the same distances as indicated at the ends of seismograms. Scattered waves have more high frequencies and are of shorter duration than the surface waves. The major difference is in the excitation of the fundamental mode. The fundamental mode excited by the source does not excite the scatterers as well at high frequencies as do the higher modes. This is a function of the eigenfunction distribution with depth.

Figure 4 examines the effect of wave type conversion on scattering. In this figure and those that follow, the number of kilometers indicates the total scattering distance, i.e. the distance from the source to the scatterer plus the distance from the scatterer to the receiver. The distance from the source to the receiver is fixed at 100 km. The angle in degrees is the location of the scatterer on an ellipse which has the source and the receiver at its foci and the coordinate origin at its center. Zero degrees indicate the scatterer is behind the receiver, and 90 degrees indicate that the scatterer is equidistant from the source and receiver. Three different components: vertical Z, radial R (with respect to source-receiver coordinate), and the tangential T are also indicated. In each pair of traces of Figure 4, the lower one includes the wave type conversion and the upper one does not. For each distance, each pair of traces is plotted using the same scale. From this comparison, we find that the wave type conversion is not obvious except at short distance for wide angle scattering. The Z component seems to be more independent of this effect than the other components. Thus it is concluded that the wave type conversion is important only for the horizontal components at short distances. It is at these distances that wide angle scattering occurs. For large scattering distances relative to the source-receiver distance, backscattering is all that occurs from the the geometry.

Figure 5 illustrates the effect of mode conversion. Three cases are displayed in which the number of modes permitted to be converted to other near neighboring modes are 1, 5 and 10. In addition, the effects of wavetype conversion are also shown. The scattered waveforms are created by combining the effect of seven scatterers evenly distributed on the ellipse defined by the scattering distances. The amplitude scale of plotting for every scattering distance is the same. As in Figure 4, the Z component seems stable and does not accumulate as much contribution from other modes except at the short distance where mode conversion must still be considered. On the other hand, the R and T components (Figures 5b and 5c) are sensitive to the number

of modes allowed to convert each other and to the wave type conversion. A low mode, low frequency motion can be seen (Figures 5b and 5c), which is caused by the conversion of higher modes to lower modes during the scattering. These results do not support the diagonal selection rule, although the use of it alone will not cause major differences in the coda excitation For the elastic medium, the energy exchange by the mode conversion is important especially for the two horizontal components. The mode conversion can be looked upon analagous to a change of incident angle on the layered medium after scattering. It describes the effect similar to the scattering pattern for body body wave illustrated in Aki and Richards (1980, chap 13). Figure 6 is a similar display as Figure 5 but for an explosive source with the scattering distance at 110 km. A noticeable tangential component is obtained which is simply a result of scatterer geometry. Mode conversion and wave type conversion are both important at this scattering distance.

The location of the scatterer at different positions with respect to the source and the receiver is important in exciting the scattered wave. Figure 7 is for scatterers at different locations on an ellipse at scattering distances of 110, 300, and 500 km. The amplitude of each trace is normalized to the same distance using a $1/r^m$ ($m=1.0$) rule which will be discussed later. In these figures, waves from three different double-couple sources are summed to average out the radiation pattern effect. We can see that the amplitude changes along different azimuth. An amplitude relation between R and T components is observed, e.g., when R is large T is small. It is worth noting that a scatterer close to the source or the receiver is not necessary to create large scattering. From the variation of amplitudes around the ellipse, we can see an averaged effect of scattering pattern.

We next examine the effect at different vertical depths. A result is shown in Figure 8. The displays are for scatterers at the distances 200 km (Figure 8a) and 500 km (Figure 8b). The effect of two source depth 10 km and 25 km corresponding to the

upper and lower sets of traces are shown. A Q model 10U0.5Q, which will be explained later, is also applied. It is found that the scatterer at greater depth preferentially excites the scattered waves with the higher phase velocities. The scatterer in the upper sedimentary layer (0.5 km) is capable of generating well dispersed, long duration scattering waves. Because of dissipative attenuation, the shallow scatterers yield waveforms that lose their energy and frequency content faster, which makes them more comparable to the the effect of deeper scatterers. At larger propagation distances, the difference between scattered waves at different depths is gradually reduced, although the effect of attenuation may still be seen. In Figure 8b, we can see that the high frequency components are attenuated for shallow scatterers where Q is low after traveling long distance. But their amplitudes and waveforms are not too much different except for the low frequency fundamental mode. This indicates that a scatterer at any depth in the crust generates a similar scattered signal.

Numerical experiment II: Scattering Q and Intrinsic Q

As shown in the previous section, the scattering coefficient is a function of the correlation between scatterers, the inhomogeneity size, and the incident wave length. To make the problem easier to solve, we defined a scattering attenuation unit (U_{ss}) from which we obtained the scattering coefficient α after taking into account the angular scattering variation. The amplitude decay is given by $e^{-\alpha r/2}$ where r is the scattering distance. In fact, this is a definition of turbidity which is used to describe the scattering energy loss mechanism (Dainty, 1981). In our model, the scattering attenuation is assumed the same for different scatterers which are distributed randomly and uniformly along scattering wave path passing through them. We will examine the effect of scattering on the wave energy loss and compare this with the attenuation due to anelastic absorption. The anelastic attenuation is calculated by perturbing the elastic constants and combining with the intrinsic Q values.

Figure 9 shows the effect of different levels of scattering attenuation from scatterers at a 5 km depth and a 110 km scattering distance. Three plots, a, b, and c correspond to 10, 100, and 1000 scattering units (U_{ss}). It is found that high frequency signals are just partially absorbed for different U_{ss} values at this short propagation distance. The effect of scattering attenuation seems to broaden the pulse, i.e., redistribute the wave energy over longer time range.

Figure 10 shows an example with scattering distance extended to 300 km. Figure 10a is for the scatterers at 5 km depth and 10b for the scatterers at 0.5 km depth. The uppermost trace in this figure is the reference trace which does not involve any Q effect. Other traces are named by the symbol pUqQ which is read as scattering Q having p U_{ss} and intrinsic Q having values from the model q. The basic Q model used is $Q_\beta = 300$ for upper 20 km and 2000 for the rest in the CUS model. 2Q indicates twice as much attenuation as 1Q, e.g., Q_β=150. It is obvious that the scattering Q reduces the high frequency energy less than intrinsic Q. This means that the scattering Q is not too sensitive to the scattering environment. If the anelastic part of structure does not dissipate all high frequency signal, the scattering Q may not reduce it even under strong scattering conditions. Furthermore the scattering Q reduces the scattered pulse amplitude but does not affect its frequency content much as can be seen from the traces in 10U0Q and 40U0Q. In Figure 10b, we also find that the scattering Q seems to suppress the lower mode signals and enhance the high frequency higher modes. However, this feature probably depends on the velocity model used. From this test, we conclude that the effect of scattering Q and intrinsic Q are apparently different.

If the scattered arrivals from different distances constitute the coda at different lapse time, the frequency content of these pulses may indicate the effect of Q at different places of coda. To examine this effect, we generate the scattered pulses at two distances: 200 km and 500 km under different Q conditions. These are shown in

Figures 11 and 12. The Parts a and b are for the scatterer depths at 5 km and 15 km at these depths the Q_β values are different. The spectra of the traces are also plotted, shifted by a factor of ten for clarity. One thing revealed from this test is that the scattering attenuation absorbs the high frequency signal equally well irrespective of the scattering distance or the scatterer depth. This is shown by the difference in the slopes between the first and the second spectra. This is due to the fact that a similar scattering environment is assumed when calculating scattering coefficient α. The intrinsic Q, on the other hand, attenuates the high frequency signals rapidly for the shallower scatterer where intrinsic Q is low. Figures 12a and 12b can be thought of as two extreme cases: in 12a intrinsic Q dominates, and in 12b scattering Q dominates. The final Q value must result from the interaction of these two attenuation mechanisms. If the data show a strong frequency dependence at high frequency range, it is possible this is the attenuation from deep structure and the effect of scattering Q prevails. At the low frequency (<1 Hz), it is difficult to tell the difference between these two mechanisms.

Numerical Experiment III: Geometrical Spreading

Aki (1969) proposed a scattering theory which describes the coda waves of a local event as being composed of backscattered waves from many random distributed inhomogeneities in the lithosphere. A relation from his model, which has been widely used in the literature, is

$$A(\omega\,|t) = C(\omega)t^{-\nu}e^{-\omega t/2Q_c}$$

where $A(\omega\,|t)$ is the average peak-to-peak amplitude around the frequency ω and the time t, $C(\omega)$ is the coda shape function which includes the scattered wave excitation term and a dispersion correction, $t^{-\nu}$ is for geometrical spreading, and the exponential term describes the dissipative attenuation. The value of ν is taken as 1.0 for body waves, 0.5 for surface waves, and 0.75 for a diffusion model (Aki and Chouet, 1976).

Treating coda of local earthquakes (distance < 100 km), the source and the receiver are set at the same place to simplify the calculation of backscattering time in this model. Sato (1977) proposed a modification of the geometrical spreading factor for near scatterers which create waves arriving at the receiver just after the direct wave. This modification takes into account the separation between the source and the receiver and is used for regional earthquakes (Pulli, 1984). Kopnichev (1977) also derived a similar correction by considering the ellipticity of the scatterer surface for arrivals at a given time. In fact, this correction represents a geometrical change of the scatterer distribution ranging from a flattened ellipsoid to a shape similar to a sphere at large distances (from an ellipse to a circle for surface waves as illustrated in Figure 2a). It is purely a geometrical adjustment. However, as discussed in preceding sections, the scatterers at the near distances yield significant mode conversion and wave type conversion. A more complicated nature of scattered waves is expected there. Similarly, because of the importance of scattering angle in controlling the scattering mechanism (Wu, 1984), its effect must be significant at short distance where the scattering angle changes abruptly. In this section, we will measure this effect from simple nuerical studies. The result indicates that the so called 'Sato's correction' which gives a heavier geometrical spreading correction in the early part of coda than Aki's formula is still too small as the scattered wave energy changes rapidly between modes and wavetypes at near distances.

In order to see the variation of geometrical spreading factor, we generate many scattered pulses at different scattering distances , ignoring dissipative attenuation, both of intrinsic and scattering. An averaged peak-to-peak amplitude is then measured , with narrow band filtering if needed, and plotted in log-log scale with the distance. One of the results is shown in Figure 13a. The scattering distance is spacing by 10 km up to 600 km and the receiver is kept at 100 km from the source. It is obvious that there exists two slopes. A steeper slope with amplitude d·›pping rapidly with the dis-

tance is seen in the front part. A similar tendency is also observed for the tangential component (Figure 13b). In these figures, the unfiltered scattered wave (upper one) and the filtered scattered wave all follow similar trends. This is due to a similar frequency response for scattered wave even traveling over different distances (see Figure 11). Figure 14 shows a similar amplitude decay for the west United States model (Table 1). Here we have set the source-receiver distance at 300 km (Figure 14a) and at 100 km (Figure 14b). The rapid amplitude decay happens at the scatterer distances smaller than about 600 km and 200 km respectively. Hence, we may define the region with scattering distance smaller than twice the source-receiver distance as an 'unstable region' which has a rapid decrease in amplitude, and a 'stable region' at larger distances which has a spreading factor close to one. This distance separation agrees with that of 'Sato correction' of twice the source-receiver distance. Note that the decay rate in unstable region is greater than that in stable region by 0.5-1.0. This value is larger in WUS model than in CUS model (Table 1). Taking this into account, we propose a geometrical spreading correction basing on an extension of Sato's (1977) model to the surface wave:

$$\left|\frac{1}{\sqrt{\alpha^2-1}}\right|^{\frac{1}{2}} * \left(\frac{1}{\alpha^a}\,\frac{1}{2^a}+1\right) \qquad \text{for} \alpha < 2$$

where α is the ratio of lapse time on the coda to the Lg wave propagation time and a is between 0.5 and 1.0. This correction is plotted in Figure 15.

In propagating in a layered medium, not only does the amplitude of the scattered pulses decay with the distance but its duration also increases because of surface wave dispersion. Figure 16a displays the scattered pulses at different distances and Figure 16b is a linear regression which shows the rate of duration expansion. The CUS model exhibits an approximate increase in duration of 0.05 sec/km while WUS model exhibits an increase of 0.5 sec/km. Because a thicker sedimentary layer, the WUS model is said to be more dispersive. This dispersion induced pulse duration expansion must be considered when summing all pulses to form the coda.

Numerical Experiment IV: Superposition of Scattered Pulses

We have discussed the properties of a single scattered pulse. The next question is how these pulses are combined to form the coda. In this section, we will conduct an interesting experiment using the parameters determined in the preceding sections to synthesize the coda envelope. From recent studies of coda Q of regional earthquakes, Pulli (1984) and Shin and Herrmann (1985) both observed a lower Q values from the early part of coda. Der *et al.* (1984) also mentioned an obvious coherence difference between early coda and later coda. This section will attempt to propose an explanation to these observations.

From the study of scattered pulses just discussed, we make the following assumptions; 1) the shape of scattered pulse can be approximated by an exponential function te^{-at}; 2) the width of the pulse depends on its traveling distance following duration=a_0*distance ; 3) the maximum amplitude of the pulse decays as $e^{-\frac{\pi ft}{Q}}/t^m$, where the exponential term describes the effect of attenuation including intrinsic or scattering Q, and $1/t^m$ is the geometrical spreading factor; 4) the pulses arrive at the receiver in a random manner, thus the number of pulses in a time interval at any time of seismogram is assumed to be approximately constant. To take into account reasonable variation, we also allow a 10% random variation for the parameters: m (spreading factor), a_0 (duration expansion) and dtp (pulse interval). We will discuss the pulse at 1 Hz with the propagation velocity 3.5 km/sec.

With each pulse defined, the coda is then synthesized by summation of many pulses. One example of synthetic coda thus formed can be seen from Figure 16 where every individual pulse and the coda envelope after summation are plotted assuming different parameters. Since the energy of random arrivals is mixed, we use root-mean-square rule to form the coda enevlope. After constructing the coda, we then apply the Aki-Chouet's (1976) model with surface wave spreading correction , i.e., $1/t^{0.5}$, to calculate the coda Q value. The Q values at two regions, first 100 second and

the rest, are calculated separately. Here a sliding window with 10 seconds length (Pulli, 1984) is also used when taking points from the coda shape. The cases for different values of m, a_0 and dtp, which represent different scattering conditions, are examined. The coda Q values thus obtained are summaried in Table 2 when theoretical Q value is kept at 1000 and in Table 3 when Q is 150.

One astonished result revealed by this simple test is that the pulse spreading factor, m, is the most important factor which controls the coda shape decay. The duration factor and the pulse density, on the other hand, only have limited effect on the coda formation if the pulses are crowded together enough to make a smoothly decaying coda shape as usually observed. The dispersion of scattered pulses in the layered medium, which causes the duration increase, dose not affect the coda as much as first expected (Dainty, 1984). We also found that for a low Q region (Table 3) the coda decays rapidly, thus not too many pulses are needed and its Q value comes out fairly stable. The coda is said to be 'saturated' by attenuation. For high Q region (Table 2), different pulse parameter will play an important role on the coda formation.

Two different Q estimates are also observed in this test. The early part of coda always has a lower Q value. Since the pulses in the front have high amplitude and short duration and pulses in the later part are lower and longer, the decay of the coda shape composed of these pulses must be more rapid in the early part. This effect is due to pulse duration increase induced by dispersion. This is another factor affecting the early part coda shape, which makes the 'unstable region' defined before even more unstable.

As a result of repeating the above experiment for different combination of parameters m, a_0, and dtp, we obtained a prelimilary understanding of the constitution of coda by the summation of scattering waves:

1) For a high Q region, such as the eastern United States, the manner scattered pulse decay with the distance, because of geometric spreading or mode conversion,

controls the value of Q determined from coda shape. A large m value in the early part of coda (unstable region) has a major effect on Q value. This is the case predicted in Figure 17a.

2) For a low Q region, such as the western United States, the pulses which arrive at the receiver to form the coda are strongly affected by the attenuation and thus the coda shape is a stable estimator of Q. This is shown in Figure 17b.

3) The pulses with longer duration yield a longer tail which in turn leads to a higher Q estimate, but this effect is not so outstanding as expected.

4) If the pulses do mix to form the coda, the density of pulse arrivals is not very important with respect to the final coda Q values. This is due to the fact that the pulses are superposed by means of the energy which reduces the difference in the number of pulses.

5) Estimation of coda Q using only earlier parts of the coda requires knowledge of the rate of correct geometrical spreading term there.

Numerical Experiment V: Body Wave Scattering

The theory of body wave scattering in the earth has been widely discussed from the points of view of scattering from a discrete volmue (Knopoff, 1959; Wu, 1984) or superposition of scattered body waves (Sato, 1984). These theories, however, use a plane wave reacting with the scatterer in a whole space or at most a halfspace. In this section, we will discuss body wave scattering in the layered medium. The layered earth structure is an important factor which provides a circumstance for waves to react with inhomogeneities by trapping waves in the layers. We will simply extend the theory developed for surface waves, i.e., Lg waves, to body waves by using 'locked mode' approximation (Harvey, 1981). This is done by adding a rigid cap layer at great depth in the original model to trap the body waves. In doing this, the body waves become a subset of the surface-wave filed. Hence, we can easily extend the first-order

scattering theory to cover this part of scattering signals.

If the technical difficulties mentioned in the Appendix II can be overcome, the body wave scattering waveform will be generated as shown in Figure 18. Three components of ground motion with scatterer at 110 km distance and 5 km depth in the CUS model are displayed. The scattered waveform for surface wave is also plotted for comparison. As expected, the scattered waveform still resembles the shape of direct waves. Body wave scattering is strong around the P and S arrivals. This is probably caused by the P to P and P to S scattering after the P wave and S to S scattering after the S wave. The scattering from S to P seems weak. We can also see some body-wave and surface-wave scattering interaction in front of or after the main pulses. Since the amplitude of scattered body waves is much smaller than scattered surface waves, we extract the body wave scattering part by windowing and display them at a larger scale as shown in Figure 19. Results at three scattering distances are presented. The body wave scattering is complicated for this layered structure. The shear scattering is strong on the two horizontal components. Because of the compicated scattered waveform, it is easier for the generation of body wave coda especially at high frequencies after superposition of such pulses.

Next we check the body wave scattering under different attenuation condition. In Figure 20a, we plot the scattered pulses including body waves, surface waves and their spectra. The first trace is the pulses from full wave scattering, the second is a representation of the body wave part from the first trace, and the third trace is the surface wave scattered pulse which is generated by using crustal surface-wave modes only. Their spectra are plotted with the third (surface wave) two amplitude order lower. After applying Q models due to scattering attenuation or intrinsic attenuation, we obtain the attenuated scattering pulses as shown in Figures 20b and 20c. It is interesting to see that the body wave scattering suffers much less attenuation than surface wave scattering especially in high frequency range. This can be seen more

apparently in Figure 21 where spectra under different Q conditions are plotted for surface and body wave scattering respectively. Figure 21a is for scattering distance at 250 km and 21b at 500 km. In these figures the high frequency spectrum slopes do not show as much variation for body-wave scattering as for surface-wave scattering. The body-wave scattering contains higher frequencies initially and its energy is not much attenuated by either intrinsic or scattering attenuation. This might make the body wave scattering dominant at high frequencies as observed by Shin and Herrmann (1985).

Conclusion

After examing the behavior of scattered pulses generated in a layered medium, we have the following conclusions:

1) The 'diagonal selection' rule which predicts no mode conversion is not proper for scattering in the layered elastic medium. Mode conversion must be considered especially for the horizontal components or at short distances.

2) The wave type conversion between Rayleigh and Love waves, on the other hand, can be ignored except at short distances.

3) The scatterers near the surface can generate well dispersed scattered waves, but they also lose energy faster because of dissipative attenuation. The combined effct of attenuation and layering makes the scatterer depth dependence less significant.

4) The variation of scattering Q does not affect the value of apparent Q as much as the intrinsic Q. For the same scattering environment, the attenuation of high frequencies from scattering Q does not seem to depend much on the scattering location.

5) It is difficult to make a distinction between the effect of scattering Q and intrinsic Q on the final Q value.

6) Larger geometrical spreading decay is found in the early part of coda. It falls off by a factor of $t^{-0.5}$ to t^{-1} faster than the later part. The geometrical correction in the

early unstable region of coda is suggested to be larger than the simple Sato's correction. This is caused mainly by rapid mode or wave type conversion from scatterers at near distances.

7) If the scattering pulses which constitute the coda are dense enough, which is required to make a smooth decaying coda envelope, the geometrical correction factor will control the value of coda Q.

8) The body-wave scattering internally yields higher frequency arrival than the surface-wave scattering. It also suffers less attenuative absorption than the slower surface waves.

9) The effect of layering on the coda formation is very important. Because of wave trapping in the layers, even a weak scatterer distribution may create oberverable coda. This layering is the same reason that makes the Lg phase the most dominant phase in regional earthquakes seismograms.

Reference

Aki, K. (1969). Analysis of the seismic coda of local earthquakes as scattered waves, *J. Geophys. Res. 74,* 615-631.

Aki, K. (1982). Scattering and attenuation, *Bull. Seism. Soc. Am. 72,* S319-S330.

Aki, K. and B. Chouet (1975). Origin of coda waves: source attenuation and scattering effects, *J. Geophys. Res. 80,* 3322-3343.

Aki, K. and P. Richards (1980). *Quantitative Seismology: Theory and Method, Vol. I.* W. H. Freeman and Company, San Francisco, 557pp.

Anderson, D. L., A. Ben-Menahem, and C. B. Archambeau (1965). Attenuation of seismic energy in the upper mantle, *J. Geophys. Res. 70,* 1441-1448.

Bouchon, M. (1979). Discrete wave number representation of elastic wave fields in three-space dimensions, *J. Geophys. Res. 84,* 3609-3614.

Chernov, L. A. (1960), *Wave Propagation in a Random Medium,* McGraw-Hill, New York, 167pp.

Dainty, A.M. (1981). A scattering model to explain seismic Q observations in the lithosphere between 1 and 30 Hz, *Geophys. Res. Letters 11,* 1126-1128.

Dainty, A. M. (1984). Influence of Scattering on Q in the Lithosphere, *Final report to the AFSOR,* Georgia Institute of Technology, Atlanta, Georgia.

Der, Z. A., M. E. Marshall, A. O'Donnell, and T. W. McElfresh (1984). Spatial coherence structure and attenuation of the Lg phase, site effects, and the interpretation of the Lg coda, *Bull. Seism. Soc. Am., 74,* 1125-1147.

Dunkin, J. W. (1965). Computation of modal solutions in layered, elastic media at high frequencies, *Bull. Seism. Soc. Am. 55,* 335-358.

Harkrider, D. G. (1970). Surface waves in multi-layered elastic media. II. Rayleigh and Love waves from buried sources in multi-layered elastic halfspace, *Bull. Seism. Soc. Am. 60,* 1937-1987.

Harkrider, D. G. (1979). Eigenfunction normalization for energy calculations in surface wave codes (abstract), *Earthquake Notes 50,* 28.

Harvey, D. J. (1981). Seismogram synthesis using normal mode superposition: locked mode approximation, *Geophys. J. 66,* 37-69.

Herrmann, R. B. (1980). Q estimates using coda of local earthquakes, *Bull. Seism. Soc. Am. 70,* 447-468.

Hudson, J. (1977). Scattering waves in the coda of P, *Geophys. J. 43,* 359-374.

Ishimaru, A. (1977), *Wave Propagation and Scattering in Random Media,* Academic Press, New York, 250p.

Kennett, B. L. N. (1972). Seismic waves in laterally inhomogeneous media, *Geophys. J. 27,* 301-325.

Kerry, N. J. (1981). Synthesis of seismic surface waves, *Geophys. J. 64,* 425-446.

Knopoff, L. (1959). Scattering of compressional waves by spherical obstacles, *Geophysics, 24,* 30-39.

Knopoff, L. (1964). A matrix method for elastic wave problems, *Bull. Seism. Soc. Am. 67,* 431-438.

Kopnichev, Y. F. (1977). Models for the formation of the coda of the logitudinal wave, *Proc. (Dokl.) Acad. Sci. USSR, 234,* 13-15.

Malin, P. E. (1978). A first order scattering solution for modeling lunar and terrestial seismic codas, *Ph.D. Dissertation,* Princeton University.

Malin, P. E. (1980). A first-order scattering solution for modelling elastic wave codas - I. The acoustic case, *Geophys. J. 63,* 361-380.

Pulli , J. J. (1984). Attenuation of coda waves in New England, *Bill. Seism. Soc. AM., 74,* 1149-1166.

Sato,H. (1977). Energy propagation including scattering effect; single isotropic scattering, *J. Phys. Earth 25,* 27-41.

Sato,H. (1984). Attenuation and envelope formation of three-component seismograms of small local earthquakes in randomly inhomogeneous lithosphere, *J. Geophys. Res. 89,* 1221-1241.

Schawb, F.K. Nakanishi, M. Cuscito (1984). Surface-wave computation and the synthesis of theoretical seismograms at high frequencies, *Bull. Seism. Soc. Am. 74,* 1555-1578.

Shin Z. C. and R.B. Herrmann (1985). Coda wave attenuation in Eastern Canada, *submitted to BSSA for publication.*

Wang, C. Y. (1981). Wave theory for seismogram synthesis, *Ph.D. Dissertation,* Saint Louis University, St. Louis, Missouri.

Wang, C.Y. and R.B. Herrmann (1980). A numerical study of P-, SV-, and SH-wave generation in a plane layered medium, *Bull. Seism. Soc. Am. 60,* 1015-1036.

Wu, R. S. (1984). Seismic wave scattering and the small scale inhomogeneities in the lithosphere, *Ph.D. Dissertation,* Massachusetts Institute of Technology.

Wu, R.S. and K. Aki (1985). Scattering characteristucs of elastic waves by an elasteic heterogeneity, *Geophysics 50,* 582-595.

Watson,T. H. (1972). A real frequency, complex wavenumber analysis of leaking modes, *Bull. Seism. Soc. Am. 62,* 369-384.

Appendix I

I. Source Function:

For a double couple source, the source mechansim can be determined by the dip d , slip s, and strike ϕ in the following forms:

$$^{R}S = {}^{R}k\, U_r R_{ss} + \left(\frac{dU_z}{dz} + \frac{1}{2}\,{}^{R}k\, U_r\right) R_{dd} + i\left({}^{R}k\, U_z + \frac{dU_r}{dz}\right) R_{ds}$$

$$^{L}S = {}^{L}k\, U_\phi R'_{ds} - i\frac{dU_\phi}{dz} R'_{ds}$$

where

$$R_{ss} = -\sin d \cos s \sin 2\phi - \frac{1}{2}\sin 2d \sin s \cos 2\phi$$

$$R_{dd} = \sin s \sin 2d$$

$$R_{ds} = \cos 2d \sin s \sin\phi - \cos d \cos s \cos\phi$$

$$R'_{ss} = \sin d \cos s \cos 2\phi - \frac{1}{2}\sin 2d \sin s \sin 2\phi$$

$$R'_{ds} = \cos d \cos s \sin\phi + \cos 2d \sin s \cos\phi$$

For an explosive source, only the Rayleigh wave has a source function:

$$^{R}S = \frac{dU_z}{dz} - {}^{R}k\, U_r$$

$$^{L}S = 0.$$

II. Scattering angular integration:

The angular integrations for determining the scattering coefficient (Equation 6) are

$$\Theta_4 = C_0 c_2^2$$

$$\Theta_2 = A_0 a_1^2 + C_0 c_1^2 + 2C_0 c_2 c_0 + E_0(a_1 c_1 + a_0 c_2) + F_0 b_0 c_2$$

$$\Theta_0 = A_0 a_0^2 + B_0 b_0^2 + C_0 c_0^2 + D_0 a_0 b_0 + E_0 a_0 C_0 + F_0 b_0 c_0$$

where

$$A_0 = (v\rho\omega^2)^2 \qquad B_0 = ((2+v)\lambda)^2 \qquad C_0 = ((2+v)\mu)^2$$

$$D_0 = -2v(2+v)\rho\lambda\omega^2 \qquad E_0 = -2v(2+v)\rho\mu\omega^2 \qquad F_0 = 2(2+v)^2\lambda\mu$$

And a's, b's, and c's for RR conversion are

$$a_1 = U_{rm}U_{rn} \qquad a_0 = U_{zm}U_{zn}$$

$$b_0 = (k_m U_{rm} - \partial_z U_{zm})\,(k_n U_{rn} - \partial_z U_{zm})$$

$$c_2 = 2k_m U_{rm}\, k_n U_{rn} \qquad c_1 = (k_m U_{zm} + \partial_z U_{rm})(k_n U_{zn} + \partial_z U_{rn})$$

$$c_0 = 2\partial_z U_{zn}\partial_z U_{zn}$$

for RL,

$$a_1 = U_{rm}U_{\theta n} \qquad a_0 = 0$$

$$b_0 = 0$$

$$c_2 = k_m U_{rm} k_n U_{\theta n} \qquad c_1 = \partial_z U_{rm}\partial_z U_{\theta n} + k_m U_{zm}\partial_z U_{\theta n} \qquad c_0 = 0$$

for LR,

$$a_1 = U_{\theta m}U_{rn} \qquad a_0 = 0$$

$$b_0 = 0$$

$$c_2 = k_m U_{\theta m} k_n U_{rn} \qquad c_1 = \partial_z U_{\theta m}\partial_z U_{rn} + k_m U_{\theta m}\partial_z U_{zn} \qquad c_0 = 0$$

and for LL,

$$a_1 = U_{\theta m}U_{\theta n} \qquad a_0 = 0$$

$b_0 = 0$

$c_2 = k_m U_{\ell m} k_n U_{\ell n} \quad c_1 = \partial_z U_{\ell m} \partial_z U_{\ell n} \quad c_0 = 0$

Appendix II

Locked Mode Approximation

The locked mode approximation proposed by Harvey (1981) is used to synthesize body waves by surface wave normal mode theory. A rigid cap layer is placed at great depth of the original model. This acts as to trap the leaking modes and force them to become the locked modes (Watson, 1972). From normal mode theory, the imposition of this cap layer makes the branch line shrink and open a space to accept the leaking modes as they migrate from lower Riemann surfaces into the real wavenumber axis. Equivalently, this breaks down the continuous wavenumber response of body wave into discrete wavenumber spectra of surface waves.

The locked mode approximation method inherits most of the merits of surface-wave normal mode theory. The advantages of this method include:

(1) The layer response is independent of the source or receiver positions. A data file of layer response can be set up first, which takes most of computation time. The data file can then be applied to many different source and receiver configurations without repeating the calculation of layer responses.

(2) The parameters used in calculation are mostly real numbers which help in saving space and computation time. The attenuation effect can be included easily by using perturbation theor (Anderson et. al. 1965).

(3) The method can handle a wide range of frequencies, say 0.001 to 1000 Hz, as well as an arbitrary number of layers.

(4) All of the rays possibly excited in the model are automatically included. This

makes the method appropriate to use especially for complicated models and large distances. This is also the goal generalized ray theory attempts to reach.

(5) The position of pole (locked mode) is exactly known, and its contribution can be correctly calculated. This is significant compared to other wavenumber integration methods. Those methods usually use complex frequencies to shift the poles away from the integration path, i.e., real wavenumber axis before taking the direct integration (Bouchon, 1979). Since the integrand (layer response) varies very irregularly along the wavenumber axis, it is difficult, if not impossible, to find a scheme which is really efficient to sample the integration path especially for large distances or high frequencies. The locked mode theory dose not have this problem. Since it knows where the pole is, it can estimate the pole contribution exactly.

To make the 'locked mode' approximation feasible, several requirement need be fulfilled beforehand.

(1) All of the dispersion values in the frequency range of interest must be found completely. Insufficiently determined dispersion values always produce unsatisfactory results. However, the number of locked modes generated is always very large, say 1000 modes. Efficient handling of this large number of modes is an important thing in using 'locked mode' approximation. Wang and Herrmann (1980) proposed a method called jumping method which attempts to follow each pole at succeeding frequencies rather than to find them independently. This method has been proved successful especially for high frequency data. Recently, this has been further improved to prevent mode missing when the phase velocity of a mode becomes equal to a layer velocity. The dispersion curves bend abruptly at these places (Kerry, 1981). But this method is not perfect. The modes are sometimes jumped over in certain cases. After some effort, we finally realize that there may not exist a perfect pole searching scheme which can fit any kind of problem within limited computation time. To solve this

problem, an independent procedure was designed to 'patch up' the missing part based on the dispersion data already found.

(2) The pole position (dispersion value) must be located accurately. In a recent paper, Schwab *et al.* (1984) showed that dispersion values can be calculated at almost unlimited frequency by using the Knopoff (1964) matrix method. He has successfully tested Harkrider's model (Harkrider, 1970) at a frequency as high as 10,000 Hz. We do not use Knopoff's theory, instead, the conventional Dunkin (1965) compound matrix is applied but with extensive modification. Using the same model, we calculate the dispersion values and the results are as good as Schwab's. The problem of accuracy of dispersion value is now well solved.

(3) The terms which enter the final solution of normal mode theory need also be calculated accurately. These terms include eigenfunctions, amplitude factor, ellipticity, and attenuation factor (gamma). Using some analytic expressions developed by Wang (1981) following Harkrider (1980), these parameters can now be calculated very precisely. The amplitude factor which corresponds to the pole residue is a sensitive parameter difficult to determine. Rather than taking direct derivative (Harvey, 1981), it is calculated by the energy integrals (Aki and Richards, 1980, chap 7). The value of the Lagrangian can be used to judge the accuracy attained. Our results up to now have all passed this test.

There seems no theoretical difficulty for locked mode approximation method now. However, this method has an internal weakness. That is where to put the cap layer and how to remove the unwanted effects caused by it. Two erroreous phases might be generated by this artificial layer; one is the cap layer phase which is caused by real arrivals reflected from the cap layer, and the other is the truncation phase mentioned by Harvey (1981). The truncation phase arises from a phase velocity filter which is used to suppress the cap layer phase. To avoid a cap layer phase coming too

early, a deeper layer should be used for larger receiver distance. However, a deeper cap layer traps more waves or equivalently creates more modes. For example, 455 modes for 200 km cap layer becomes 1248 if the cap layer is placed at 800 km. A compromise must be set to conserve computational effort. The velocities of cap layer must also be defined carefully. They need be large to yield the desired body waves in the crust, but not too large to generate too many additional poles. Here is our experience, which can just be used as a rule of thumb. If V_c is the velocity of cap layer which is at L km depth and V_l is the layer velocity above the cap layer, a relation can be derived assuming simple reflection:

$$V_c = \frac{1+r}{1-r} V_l$$

$$L = \frac{\sqrt{r}}{1-r} R$$

r represents the reflection coefficient desired from the cap layer and R is largest distance to be used. The value of r around 0.4 is suggested, which makes V_c 2.5 times lager than V_l. and the cap layer depth grossly equals to the distance. However, if the phase velocity filtering is done properly, the distance range can be extended (at least doubled).

A proper phase velocity filter can partly smooth out the unwanted cap layer phase, but not entirely. However the phase velocity filter itself also introduces a noise caused by the trunction of filter. The truncation phase may change position and shape in the synthetic seismograms using different phase velocity filter values. Hence, it can be identified by comparing the seismograms obtained from different phase velocity filters. A frequency varying phase velocity filter, sometimes, is found useful in suppressing the truncation phase.

Figure 22 and 23 show some synthetic seismograms made from the locked mode approximation. In Figure 22, the tangential component at distances from 100 too 500 km is generated using a simplified one layer over halfspace model (SCM, Wang and Herrmann, 1980). The arrival time of each phase can be exactly identified. Figure 23

displays ten basic seismograms for the CUS model from double-couple and explosive source at a distance of 200 km. These seismogram are really of high quality.

TABLE 1

Central United States Model (CUS)

d	α	β	ρ	Q_α	Q_β
1	5.00	2.89	2.5	600	300
9	6.10	3.52	2.7	600	300
10	6.40	3.70	2.9	600	300
20	6.70	3.87	3.0	4000	2000
	8.15	4.70	3.4	4000	2000

West United States Model (WUS)

d	α	β	ρ	Q_α	Q_β
2	3.55	2.06	2.20	170	85
3	6.15	3.27	2.79	300	150
18	6.15	3.57	2.79	300	150
8	6.70	3.93	2.97	1000	500
8	6.70	3.73	2.97	1000	500
	7.80	4.41	3.35	2000	1000

TABLE 2
Q Values of Synthetic Coda
(Theoretical Q = 1000)

G.S. (m)	D.E. (a_o)	DIST=100Km			DIST=300Km		
		dtp=1	5	10	dtp=1	5	10
1.0	0.01	1116	897	717	1056	1146	1051
		1066	990	991	1025	1110	1028
	0.05	1308	1356	952	1148	1001	1263
		1091	1067	1104	1080	1133	1113
	0.1	1211	1174	1178	1215	1307	1235
		1153	1129	1089	1090	1089	1093
	0.15	1254	1373	1271	1681	1276	1470
		1161	1164	1165	1152	1140	1140
1.5	0.01	326	318	304	512	402	458
		618	628	633	652	712	645
	0.05	353	317	332	519	520	589
		643	651	662	685	682	690
	0.1	360	348	367	566	607	514
		643	657	679	698	692	721
	0.15	387	384	355	674	710	624
		652	633	702	725	723	691
2.0	0.01	202	200	196	338	304	369
		447	455	464	494	528	474
	0.05	202	195	206	342	338	354
		451	459	429	507	505	516
	0.1	208	206	203	370	375	349
		451	451	463	519	513	510
	0.15	217	205	206	428	412	458
		463	460	469	534	533	518
2.5	0.01	138	141	136	231	255	233
		348	333	343	405	377	449
	0.05	146	141	141	248	245	238
		338	348	336	398	403	394
	0.1	151	142	139	268	270	273
		348	352	361	416	411	413
	0.15	156	150	146	312	299	332
		356	357	357	423	415	427

G.S. = Geometric Spreading Factor = $1/r^m$
D.E. = Duration Expansion = $a_o r$
DIST = Scattering Distance
dtp = time interval for succeeding pulses.
In each pair, the upper number is for coda between 0 and 100 second and the lower one is for 100 and 300 second.

TABLE 3
Q Values of Synthetic Coda
(Theoretical Q = 150)

G.S. (m)	D.E. (a_0)	DIST=100Km			DIST=300Km		
		dtp=1	5	10	dtp=1	5	10
1.0	0.01	153 152	148 151	142 149	152 151	154 153	151 151
	0.05	161 160	162 159	153 160	161 161	157 162	159 161
	0.1	166 177	166 176	164 175	181 181	180 178	180 179
	0.15	177 197	175 197	174 198	217 207	221 205	226 210
1.5	0.01	115 138	114 138	112 138	132 139	123 142	128 139
	0.05	121 145	116 145	118 146	137 149	140 148	143 148
	0.1	128 159	125 161	127 162	155 167	157 165	156 170
	0.15	139 176	135 174	131 184	190 192	187 189	176 193
2.0	0.01	94 127	94 128	93 128	116 131	111 133	119 129
	0.05	96 133	95 134	97 131	120 138	120 139	122 139
	0.1	101 146	101 145	100 147	137 155	138 156	137 157
	0.15	109 162	104 163	106 162	168 178	166 177	177 179
2.5	0.01	77 117	78 116	76 117	100 123	104 120	100 127
	0.05	81 121	80 122	81 121	107 129	106 129	104 129
	0.1	86 134	82 136	81 137	122 148	126 145	120 147
	0.15	92 150	89 150	83 147	154 164	147 167	154 170

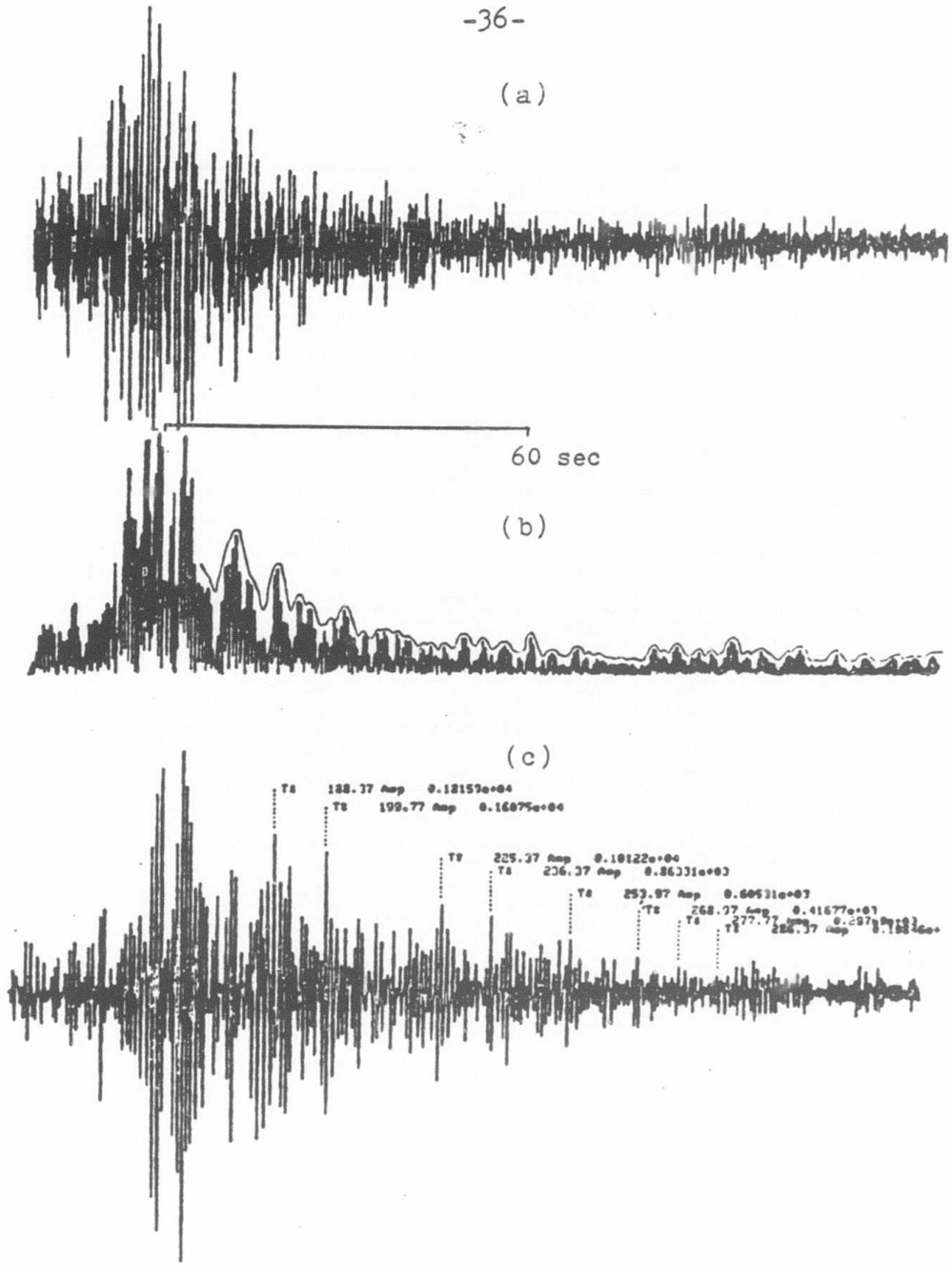

Figure 1. Observed seismograms from ECTN network. (a) is the original trace, (b) is the rectified trace, (c) is the trace narrow bandpass filtered at 1 Hz. The coda seems being composed of many small 'pulses' The coda envelope is not so uniform if examining closely. The horizontal bar indicates a 60 second time window.

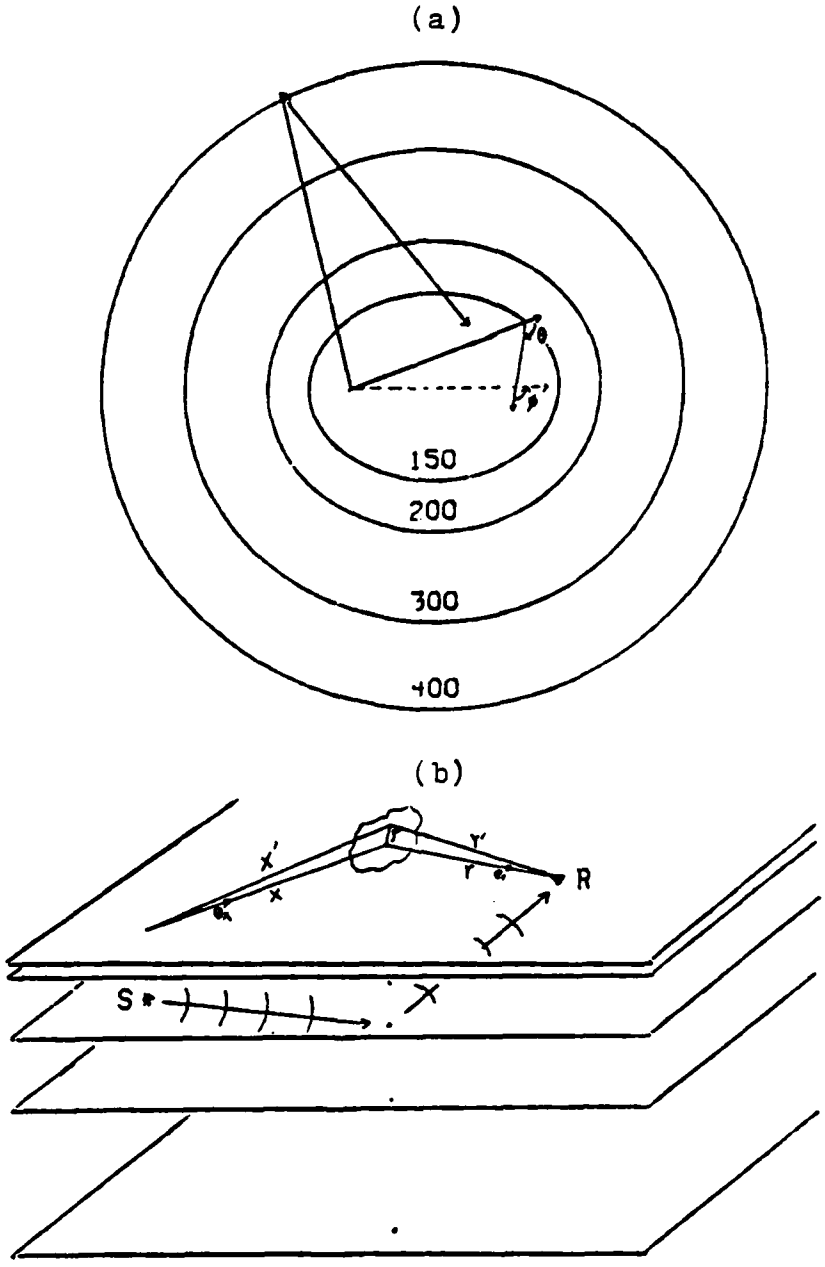

Figure 2. The scattering of waves in the layered medium. (a) is the overview with the ellipses whose major axis length is indicated by the number. The source and the receiver are separated by 100 km. (b) is the sideview. Scattering occurs in a small region within a layer.

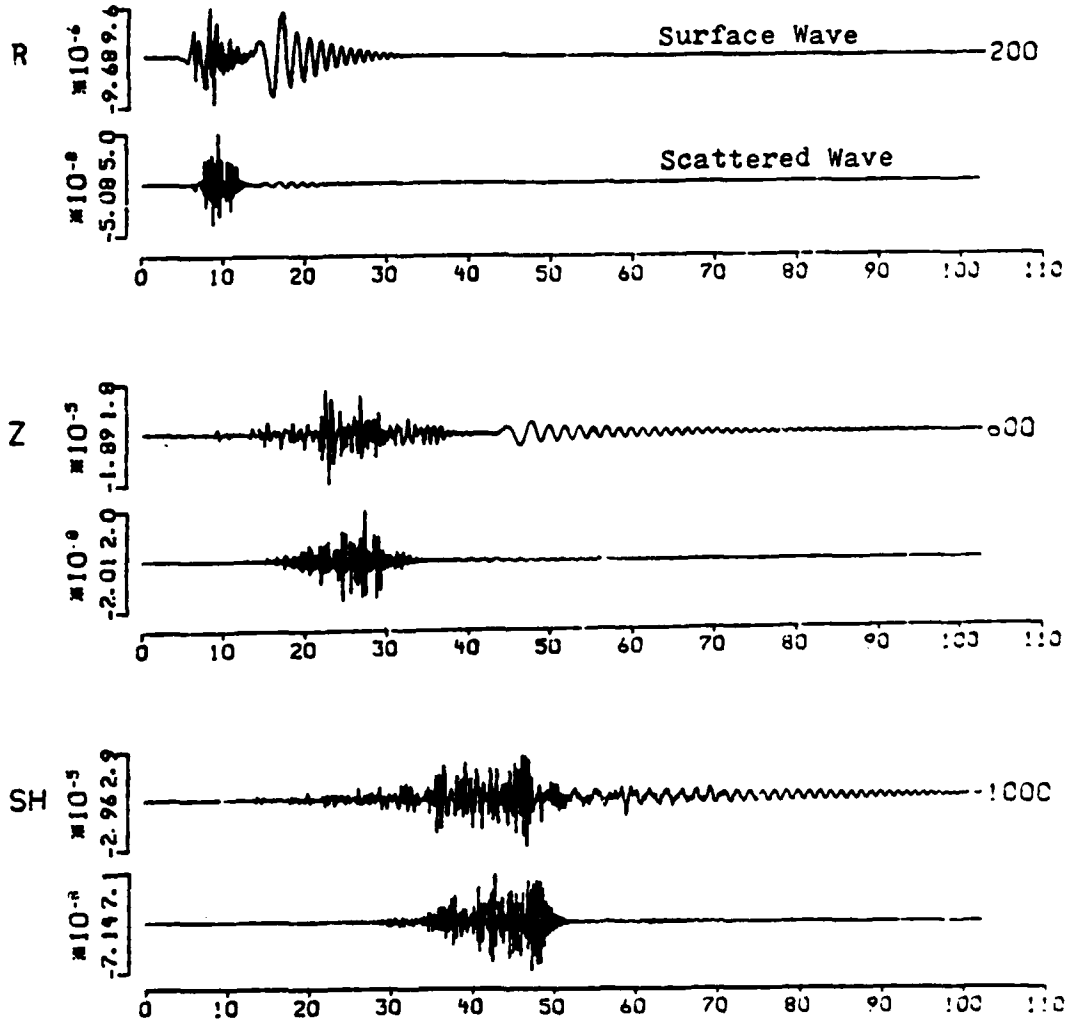

Figure 3. A comparison of waveforms of direct surface waves and the scattered waves. The numbers at the end of each seismogram indicates the source-receiver distance for surface waves and the source- scatterer-receiver distance for the scattered waves.

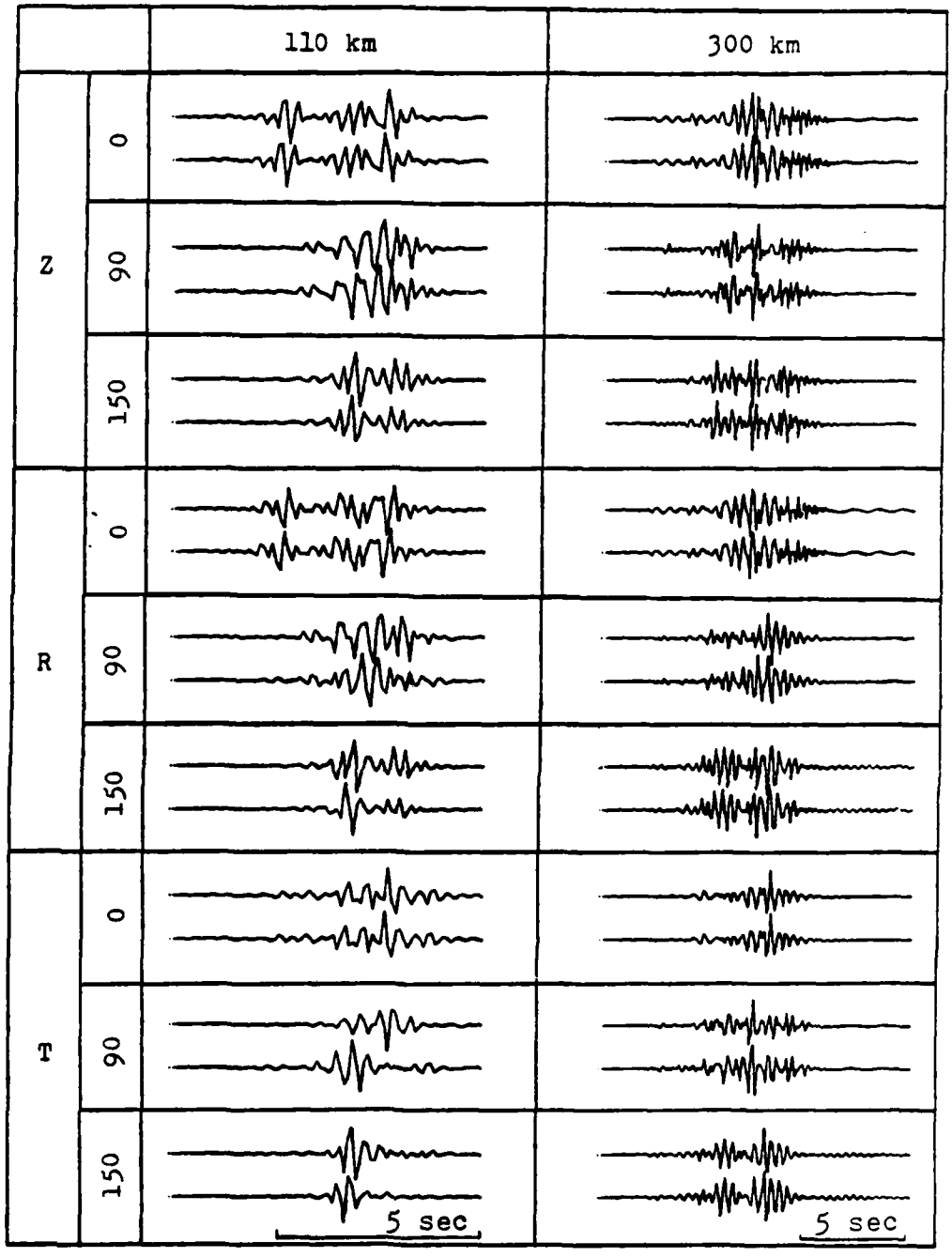

Figure 4. Wave type conversion test. The upper trace in each pair of seismograms does not include wave type conversion and the lower one does. The tests are for scatterers at the distance 110 km and 300 km, and at the angles 0, 90 and 150 degrees on an ellipse.

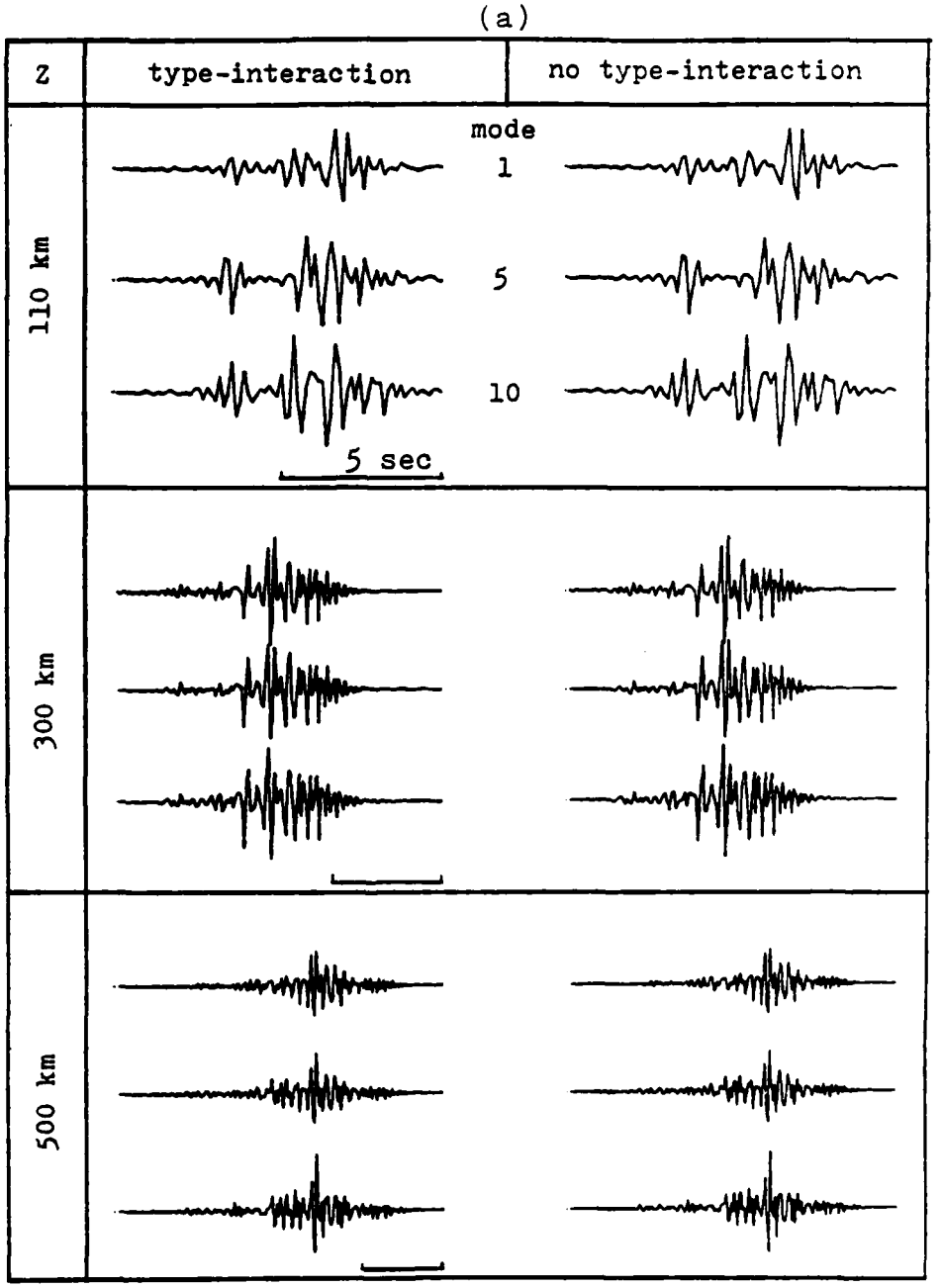

Figure 5. Mode conversion test. Cases discussed are for mode conversion permitted up to 1, 5 and 10 modes. Three scattering distances 110 km, 300 km and 500 km are included. Two columns correspond to cases with or without wave type conversion respectively. Plots a, b and c are for three different components.

(b)

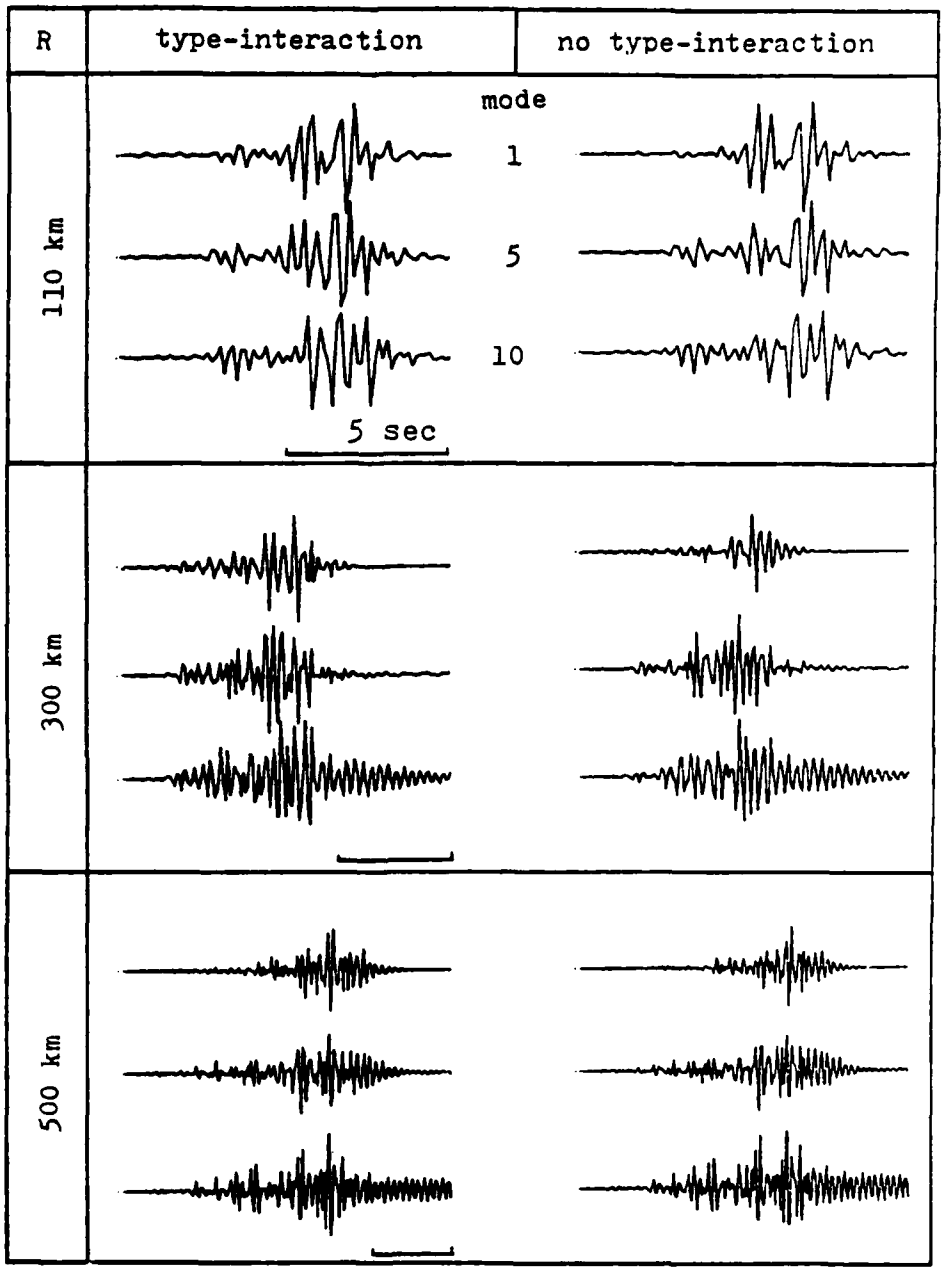
R
type-interaction
no type-interaction
mode
1
5
10
110 km
300 km
500 km
5 sec

(c)

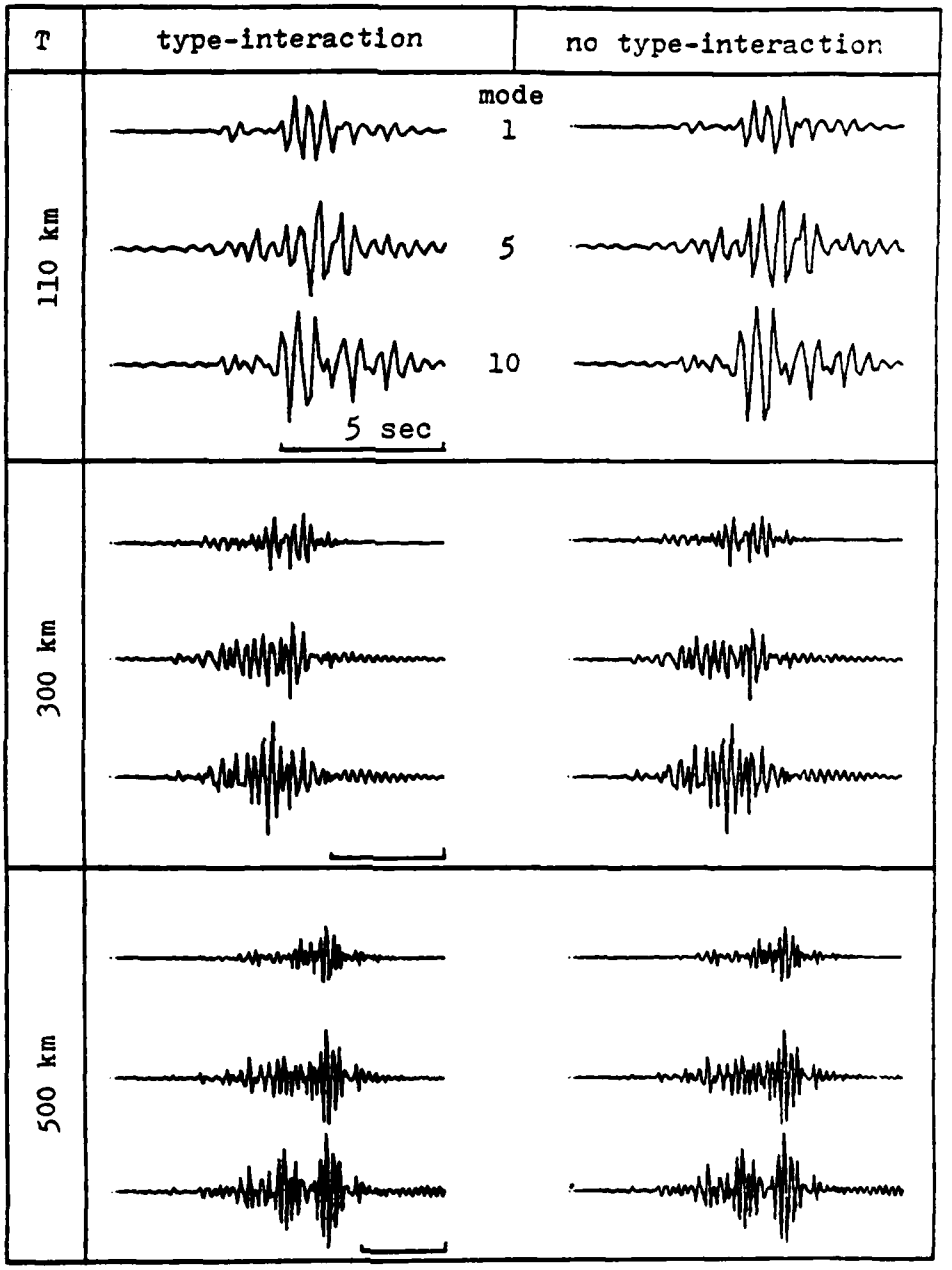
T
type-interaction
no type-interaction
mode
1
5
10
110 km
300 km
500 km
5 sec

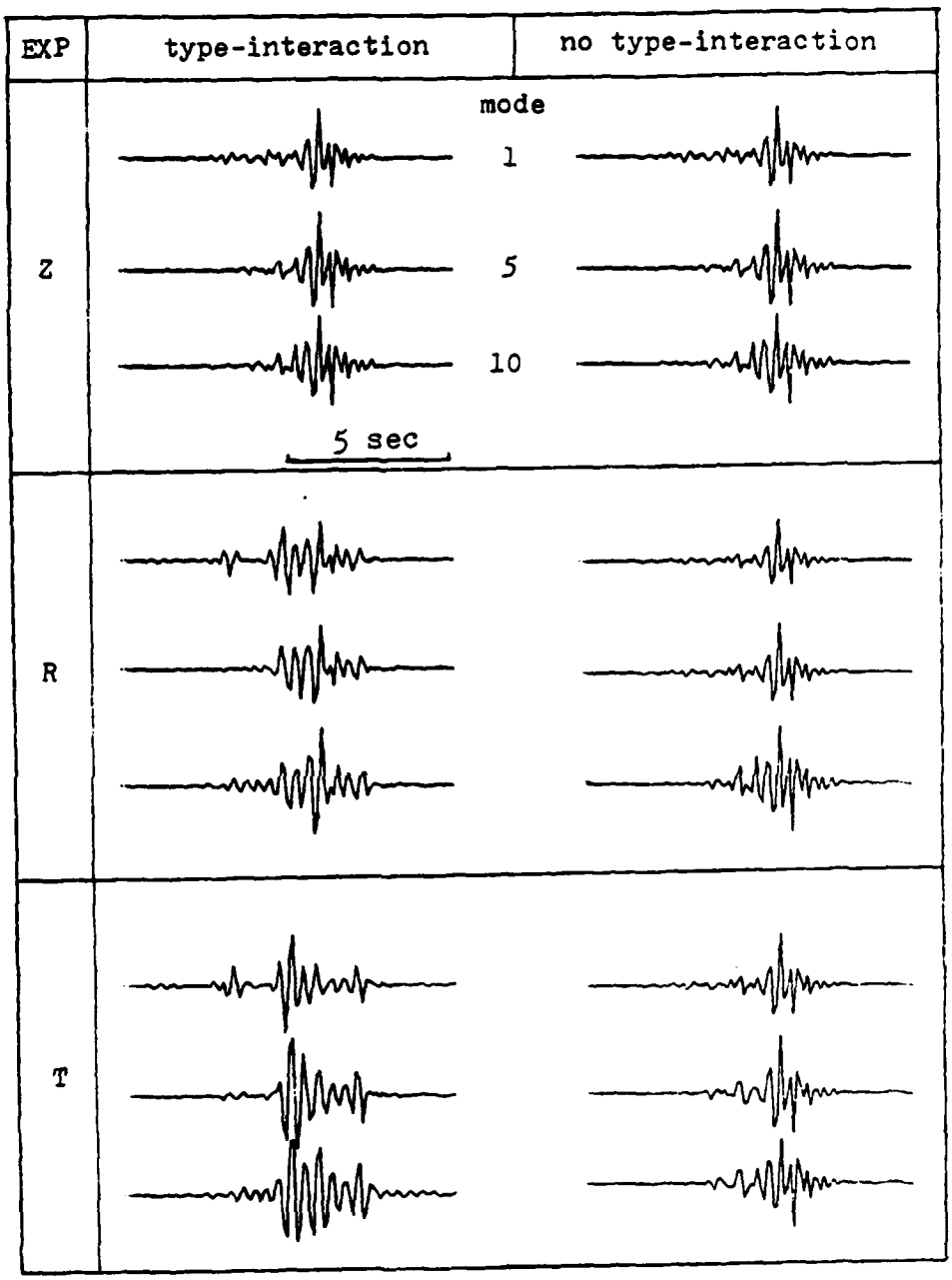

Figure 6. Mode conversion test for an explosive source. The scattering distance is at 110 km. At this distance, both mode conversion and wave type conversion are important.

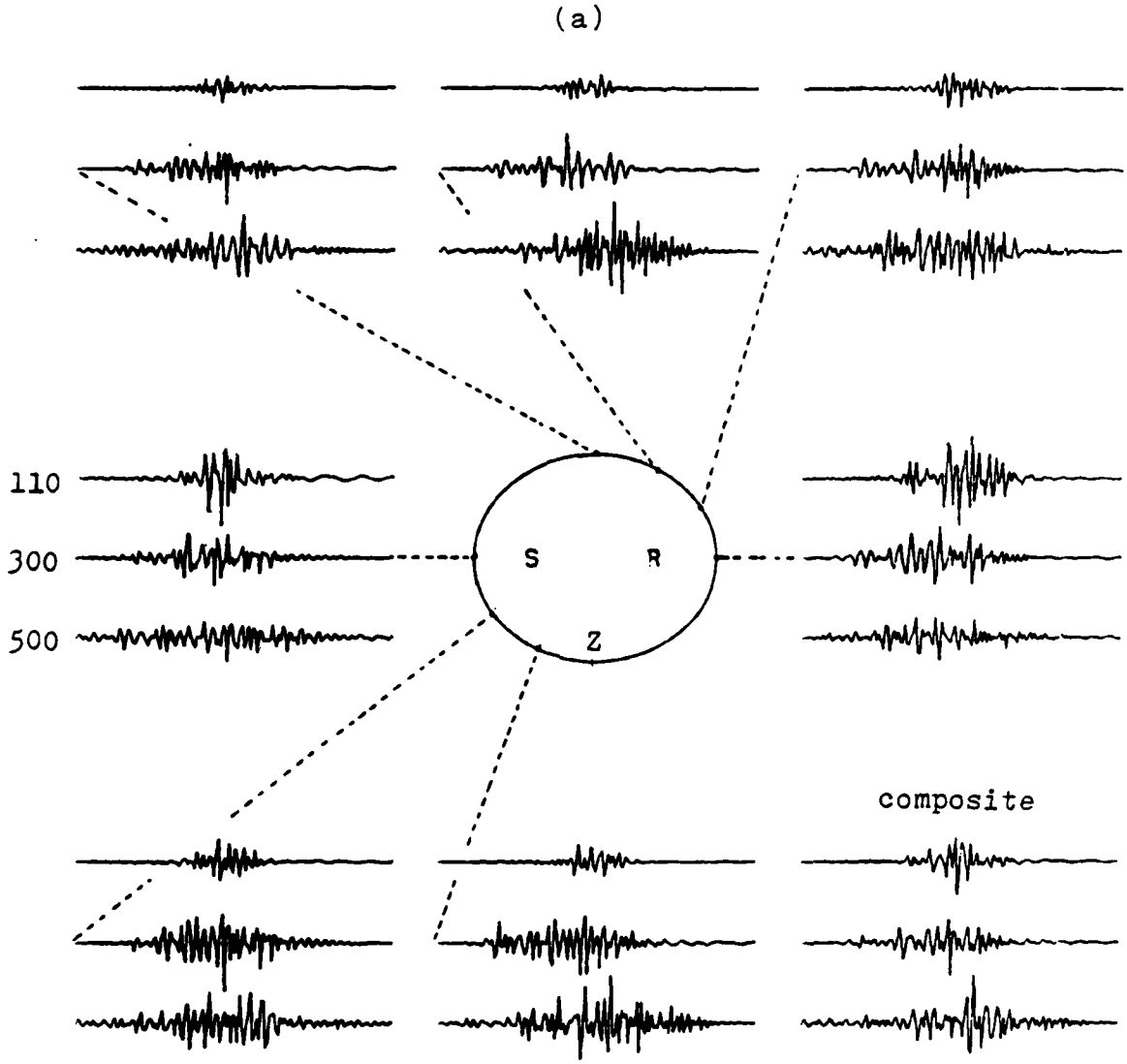

Figure 7. The effect of scattering at different location of an ellipse. Three traces at each location are for the scatterers at the distances 110 km, 300 km and 500 km with the source-receiver distance at 100 km. The amplitude of each trace has been normalized. The time span covered is 30 seconds. Plots a, b and c are for three different components.

(b)

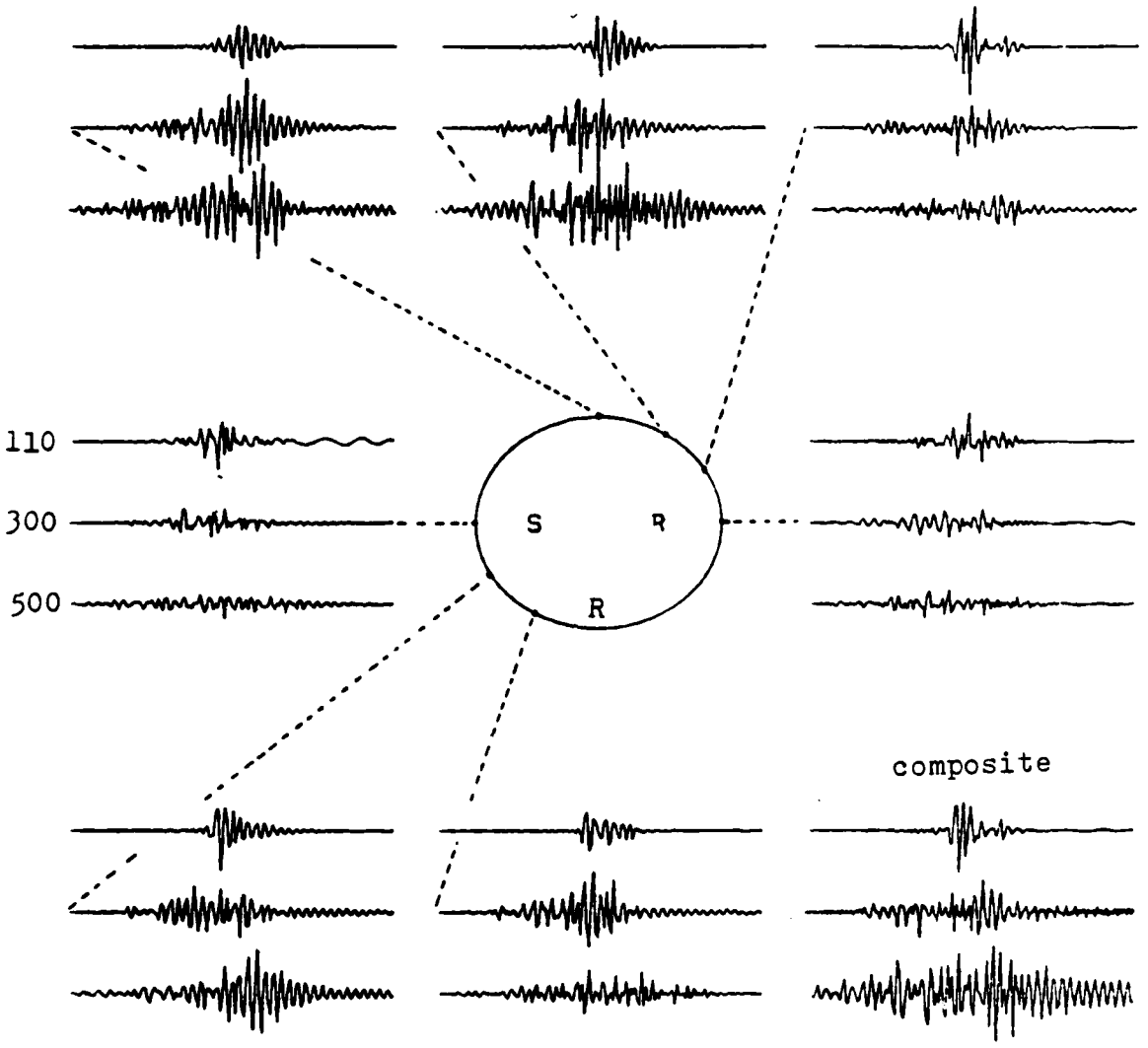

(c)

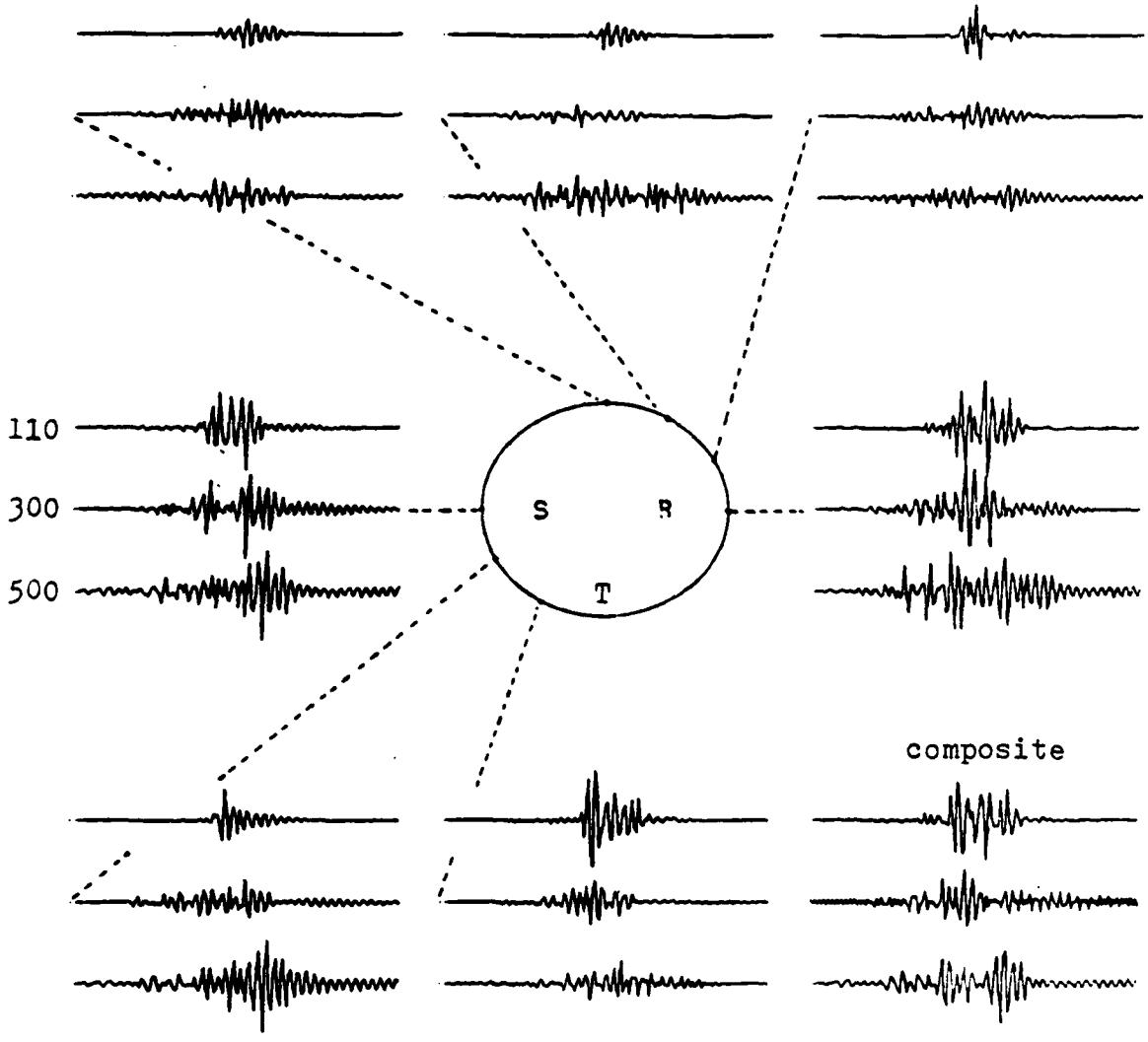

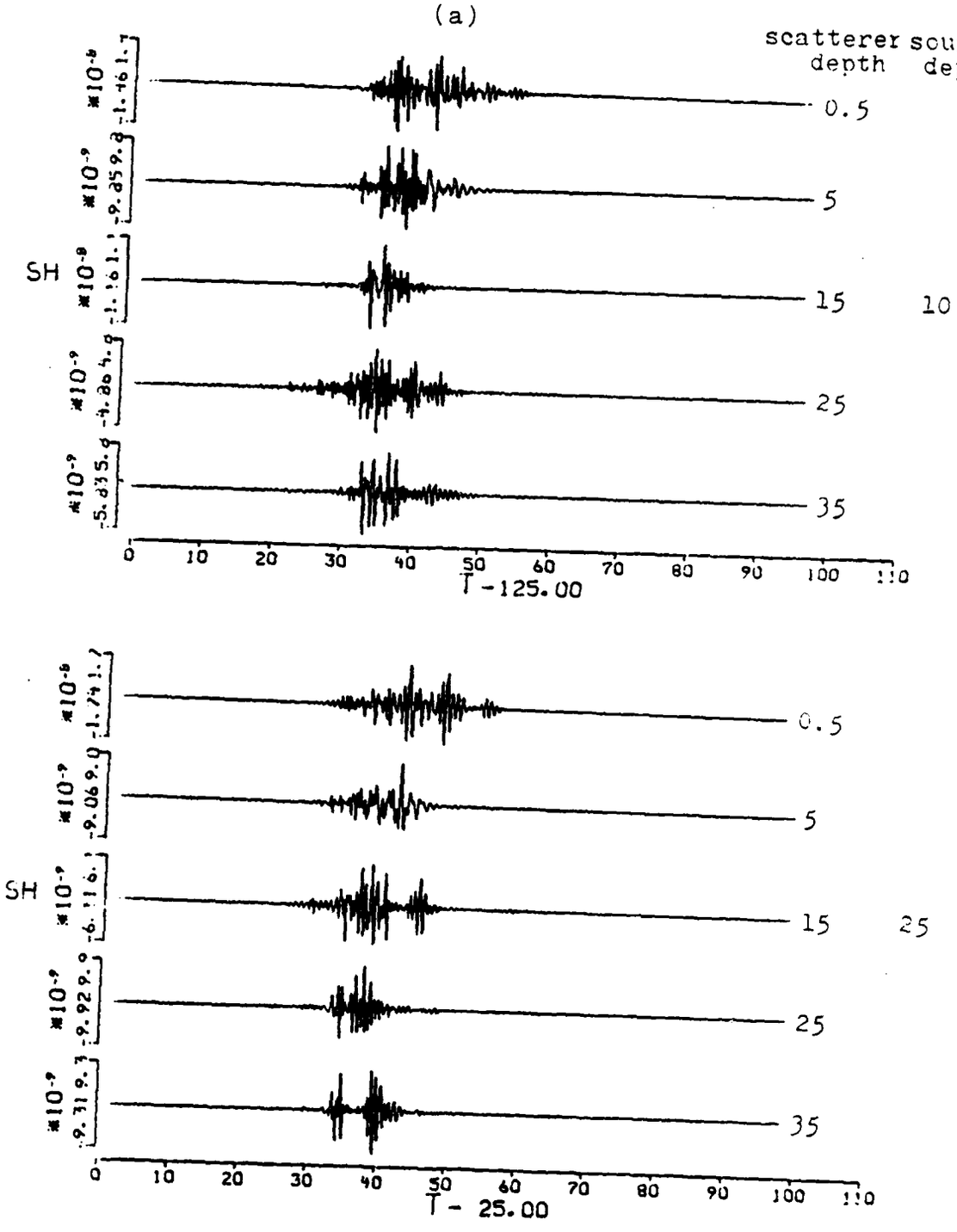

Figure 8. The effect of scatterer depth. (a) shows the tangential component with 200 km scattering distance and (b) is vertical component with scattering distance at 500 km. A Q model 10U0.5Q is also applied. The scatterers at different depths excite similar scattered pulses. The amplitudes do not differ much. This is due to the effect of the structure layering and the attenuation.

(b)

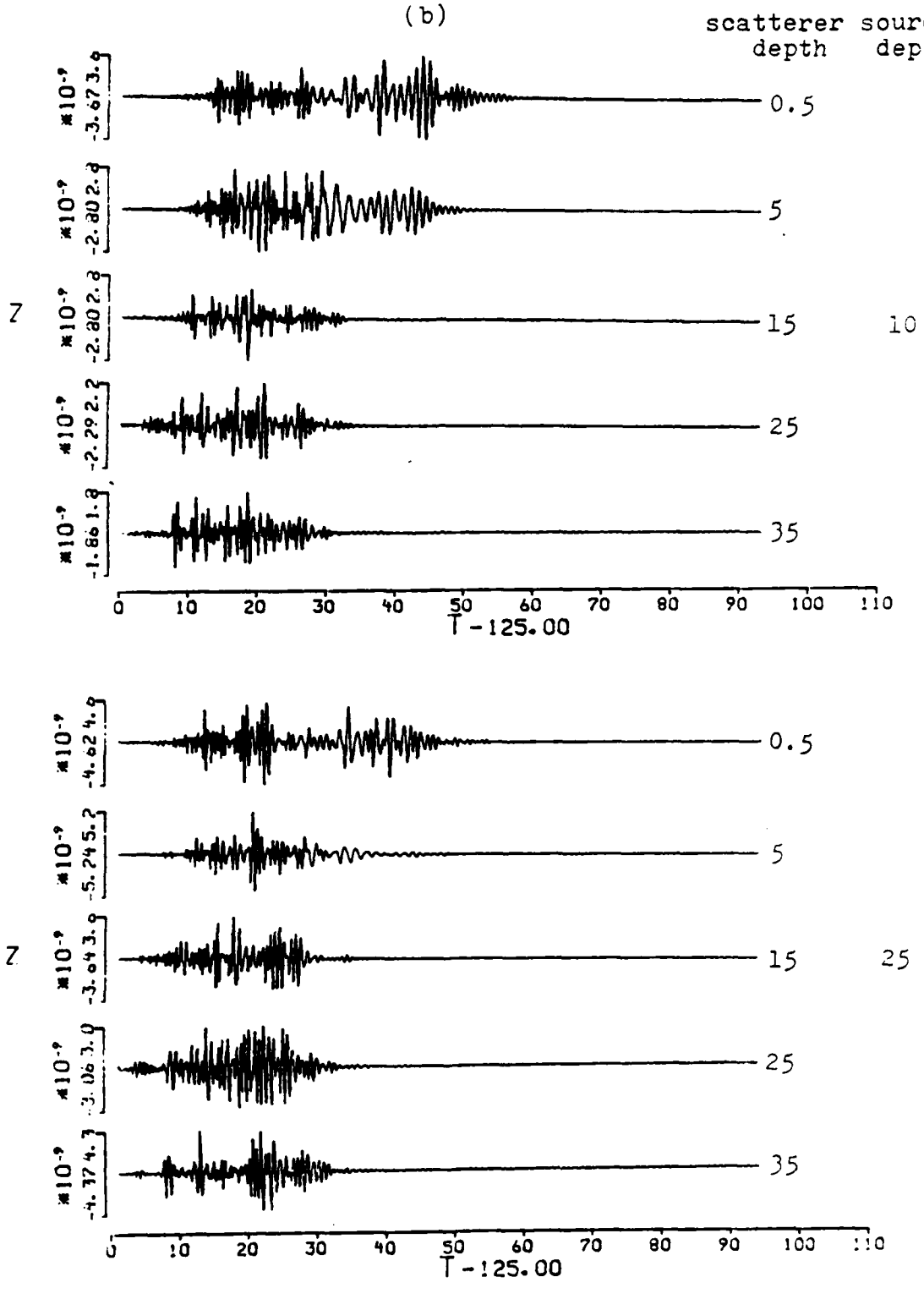
scatterer depth
source depth
0.5
5
15
25
35
10
25
Z
Z
0 10 20 30 40 50 60 70 80 90 100 110
T -125.00

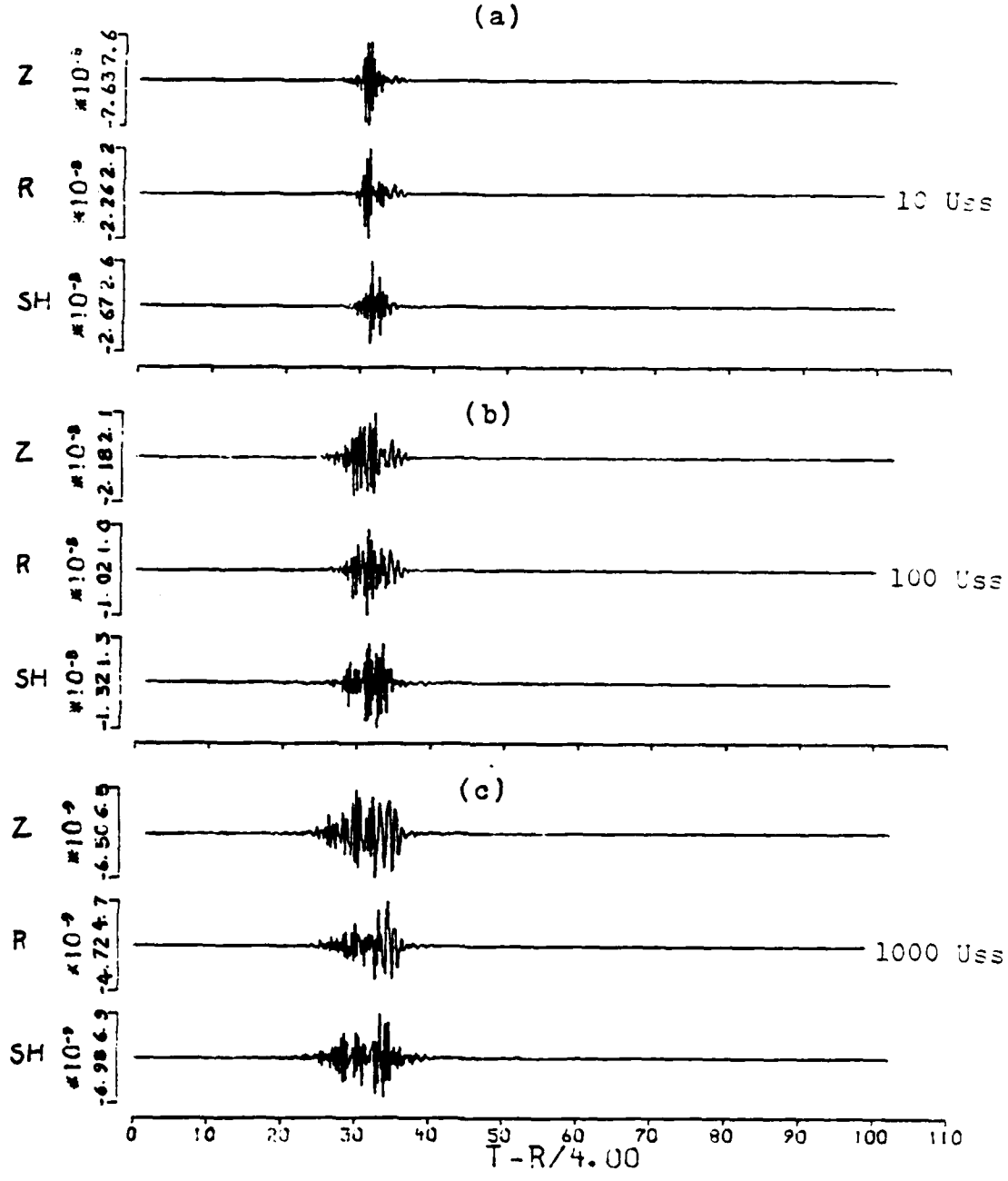

Figure 9. The effect of different degree of scattering attenuation. The scattering distance is 110 km and the scatterer is at the depth of 5 km. The source-receiver distance is 100 km. High scattering attenuation partially absorbs high frequency components and broadens the scattering pulse.

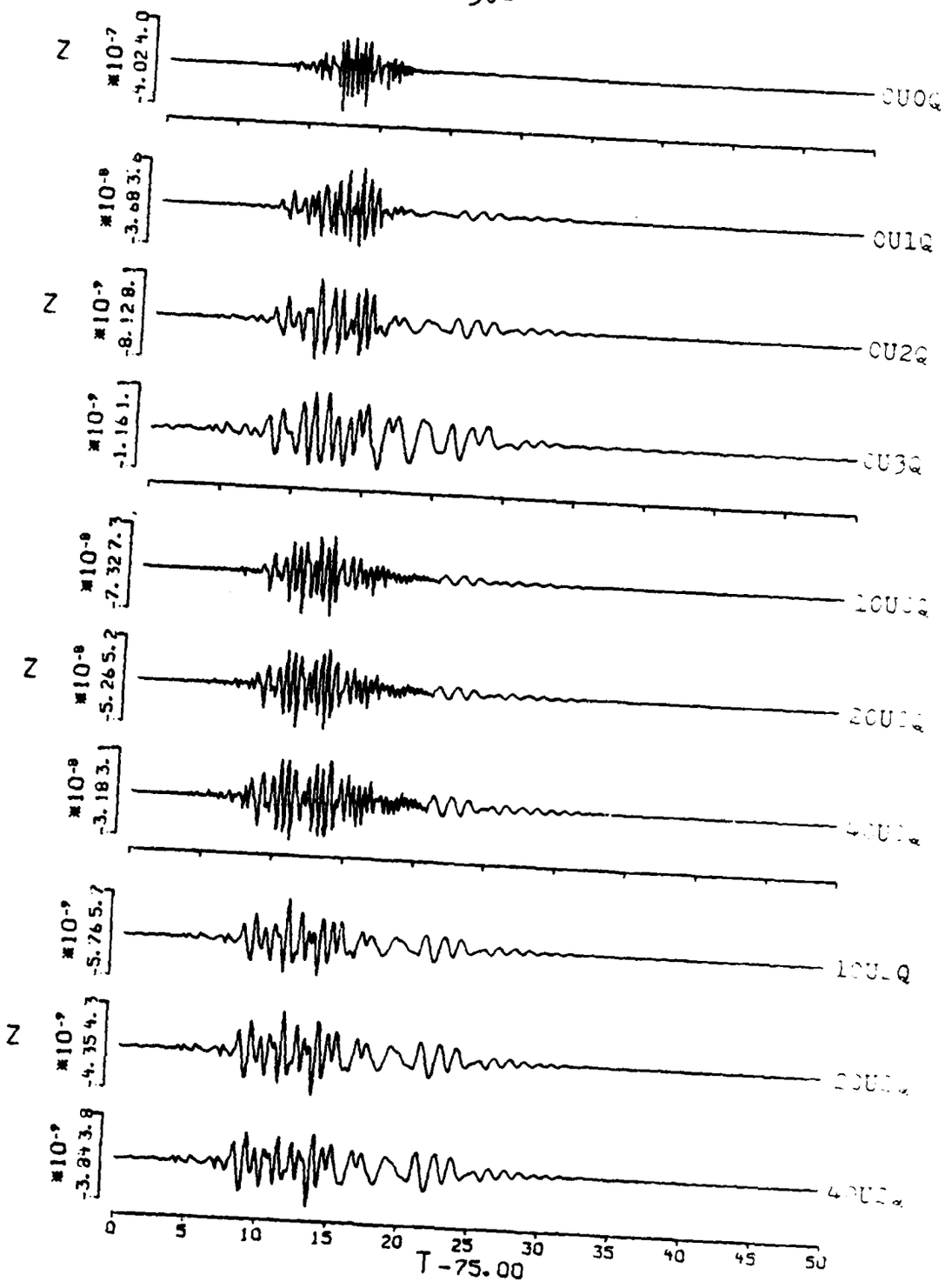

Figure 10a. A comparison of the effect of scattering Q and intrinsic Q. The scatterers are at the depth of 5 km and the scattering distance is 300 km. 10U2Q means 10 scattering attenuation unit (U_{ss}) and double anelastic attenuation as given by Q model in Table 1. Note that the frequency content of the nU0Q cases is very similar.

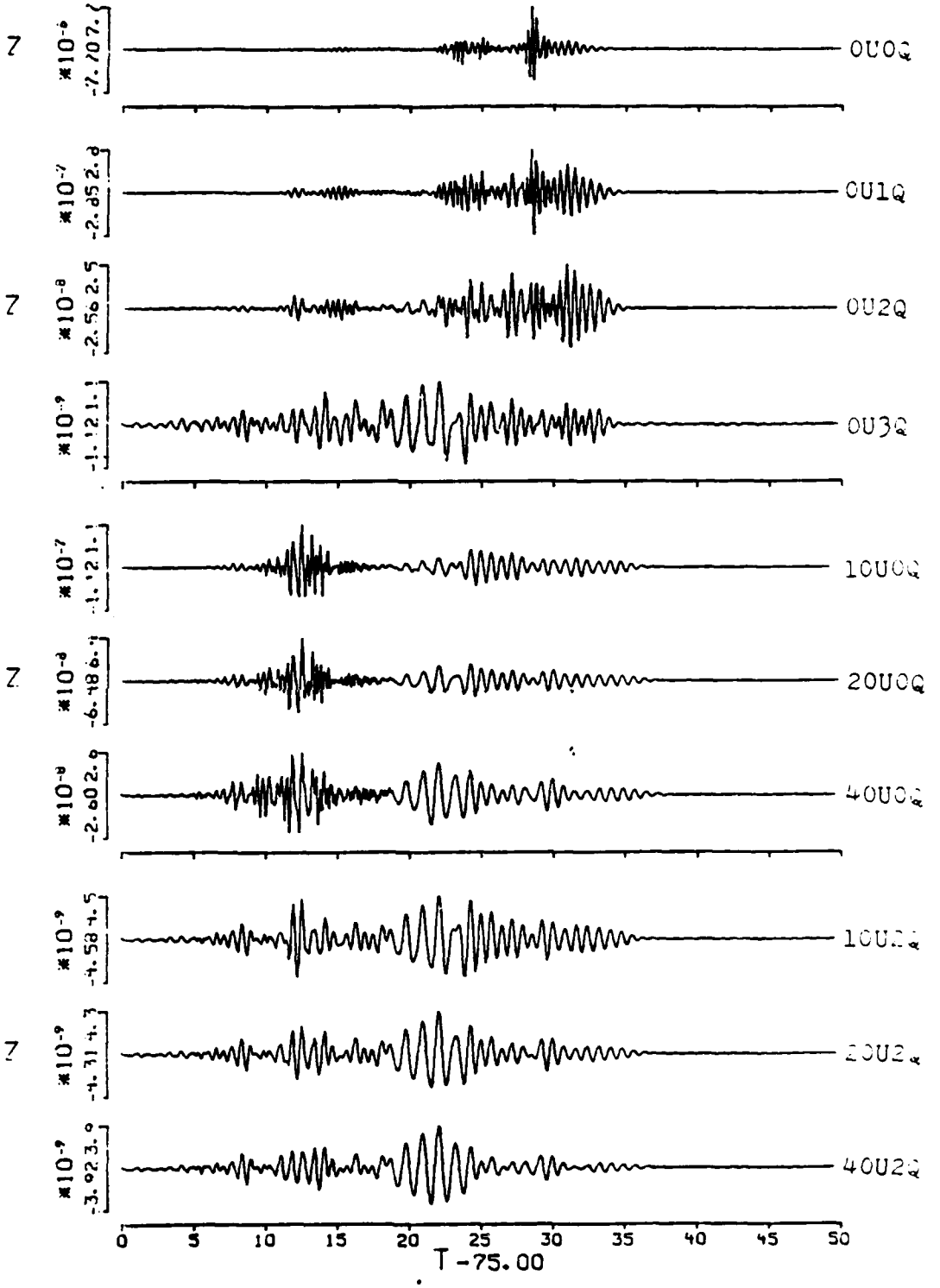

Figure 10b. Same as for Figure 11a, but for the scatterers at the depth 0.5 km. The effect of scattering Q seems to enhance the high frequency and higher mode signals.

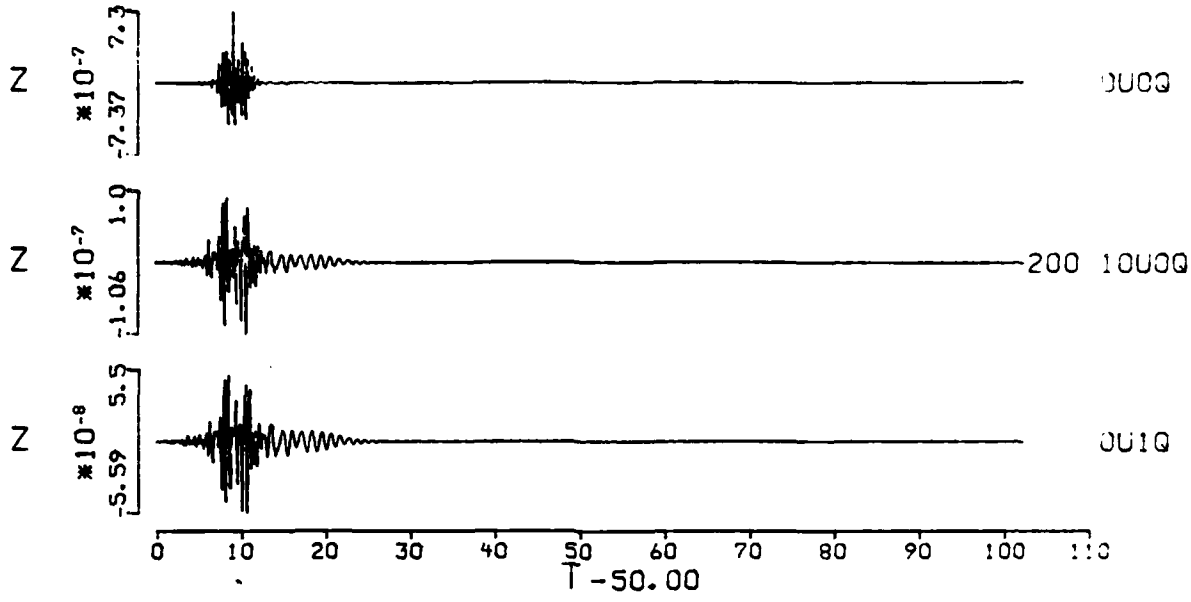

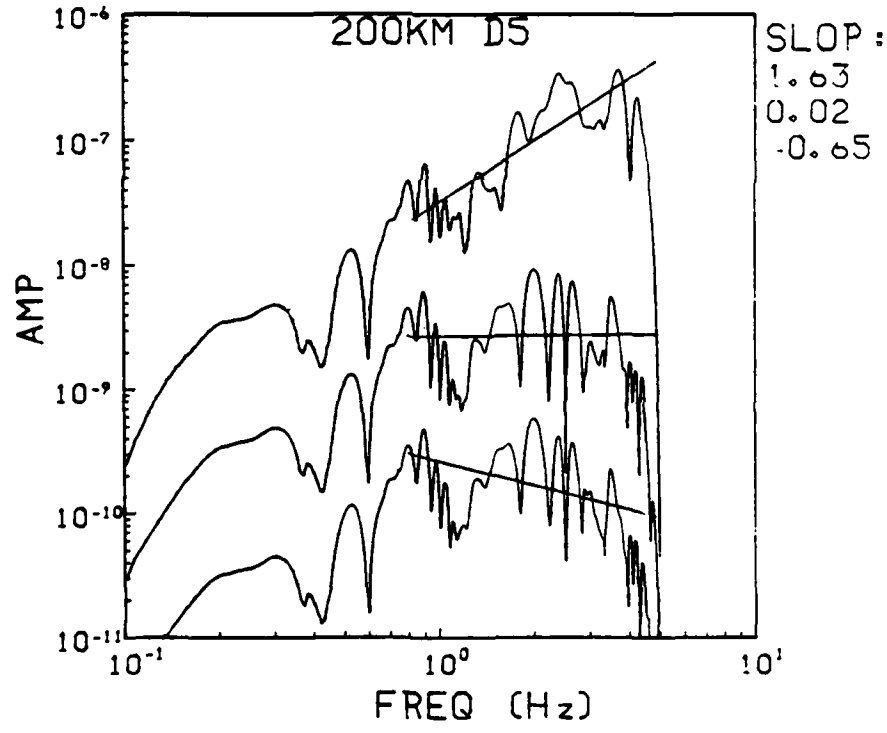

Figure 11a. The scattering waveforms and their spectra under different attenuation conditions. The scattering distance is 200 km and the scatterer is 5 km deep in CUS model. The high frequency components are attenuated equally in both cases. The spectra plotted are in the same sequence as the seismograms but shifted by a factor of ten for clarity. Their high frequency spectra slopes are also indicated.

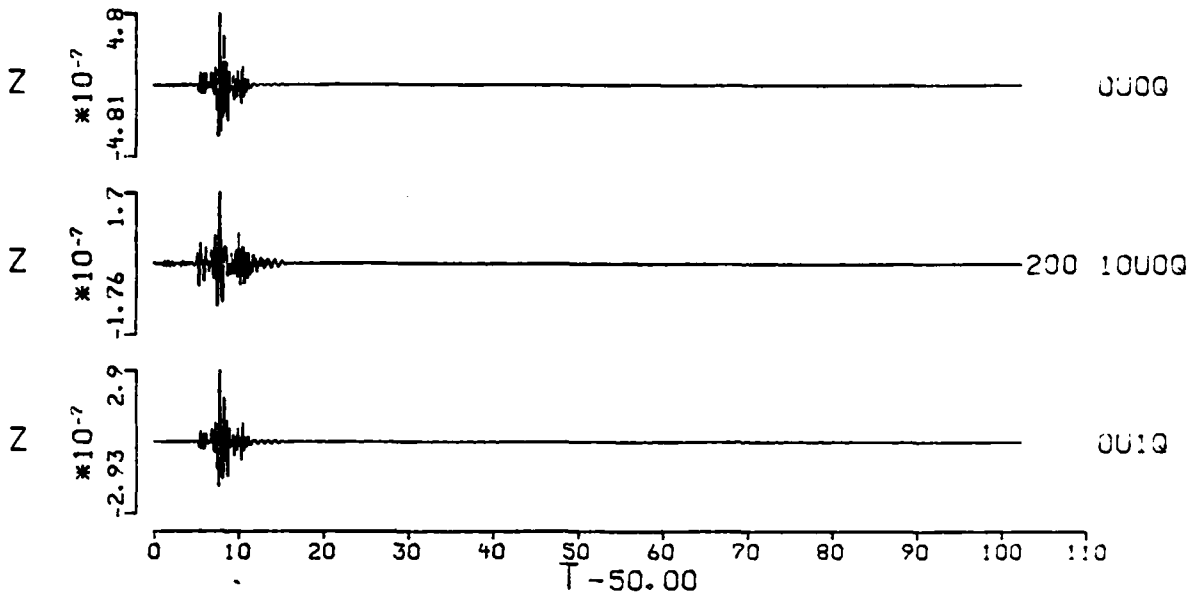

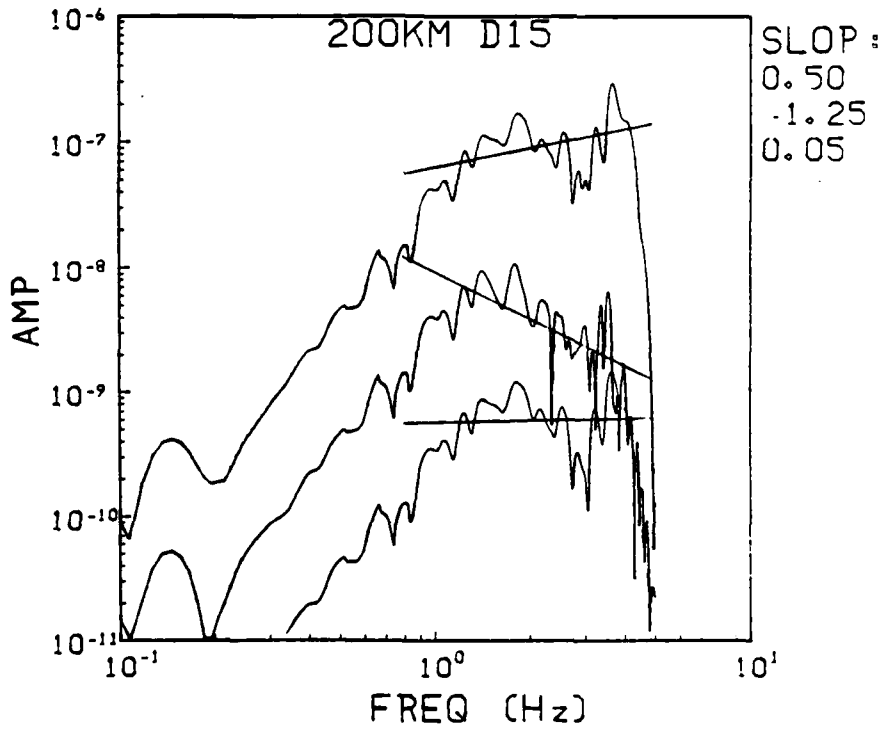

Figure 11b. Similar as for Figure 11a, but for scatterer at 15 km deep. Scattering Q absorbs the high frequencies in the main pulse. The anelastic attenuation is weaker because of the deeper scatterer.

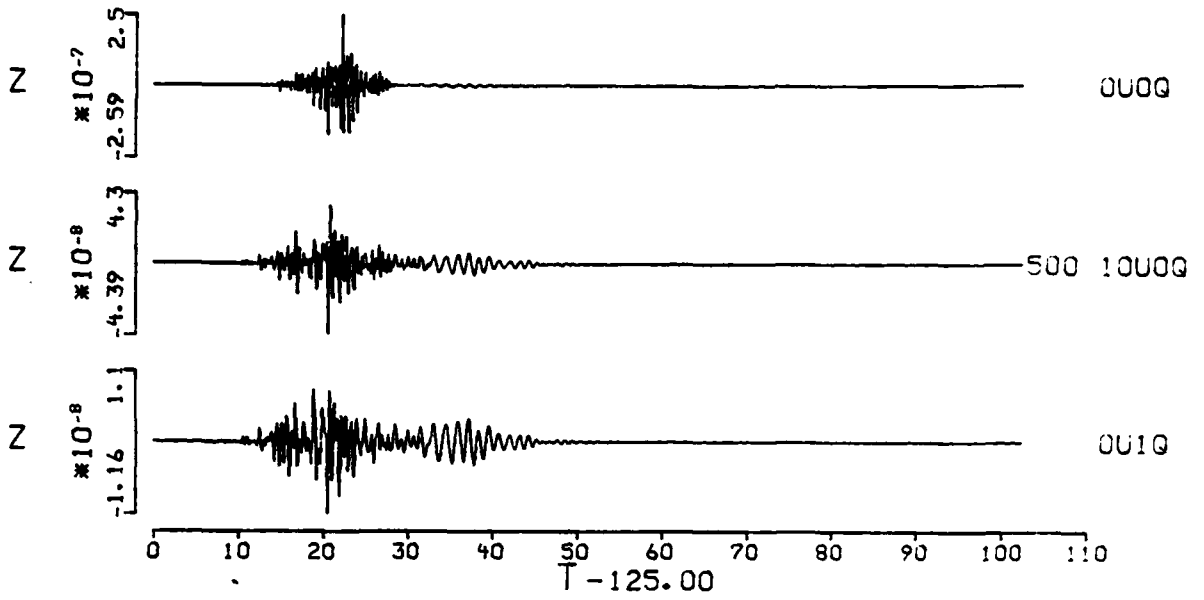

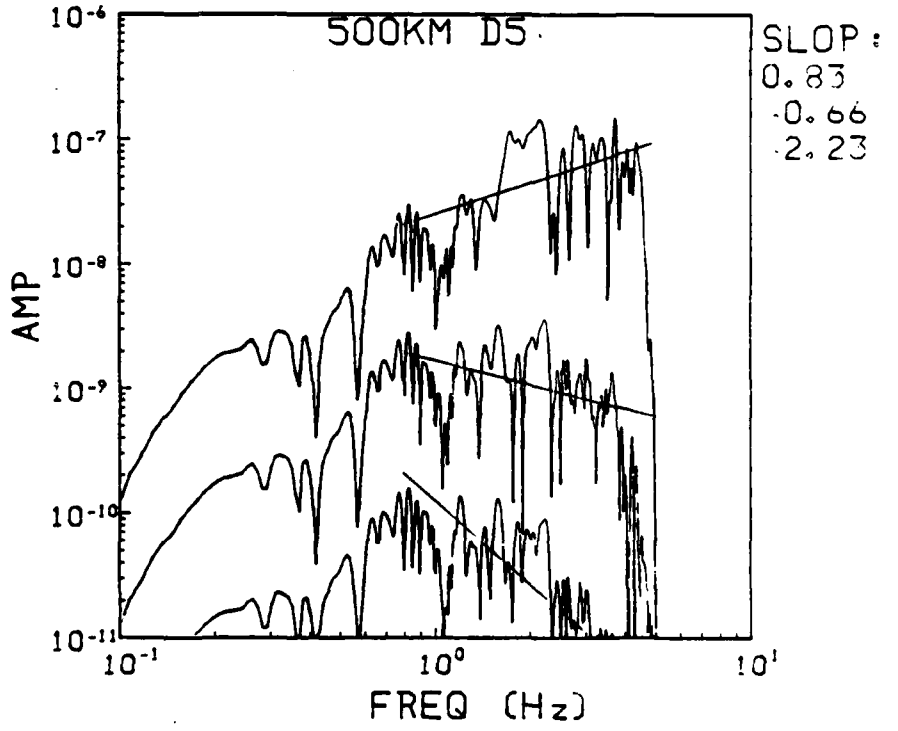

Figure 12a. A comparable case to Figure 11. The scattering distance is 500 km now. After traveling large distance, the high frequencies are absorbed especially for anelastic attenuation. In this case, the anelastic Q controls the decay of wave energy.

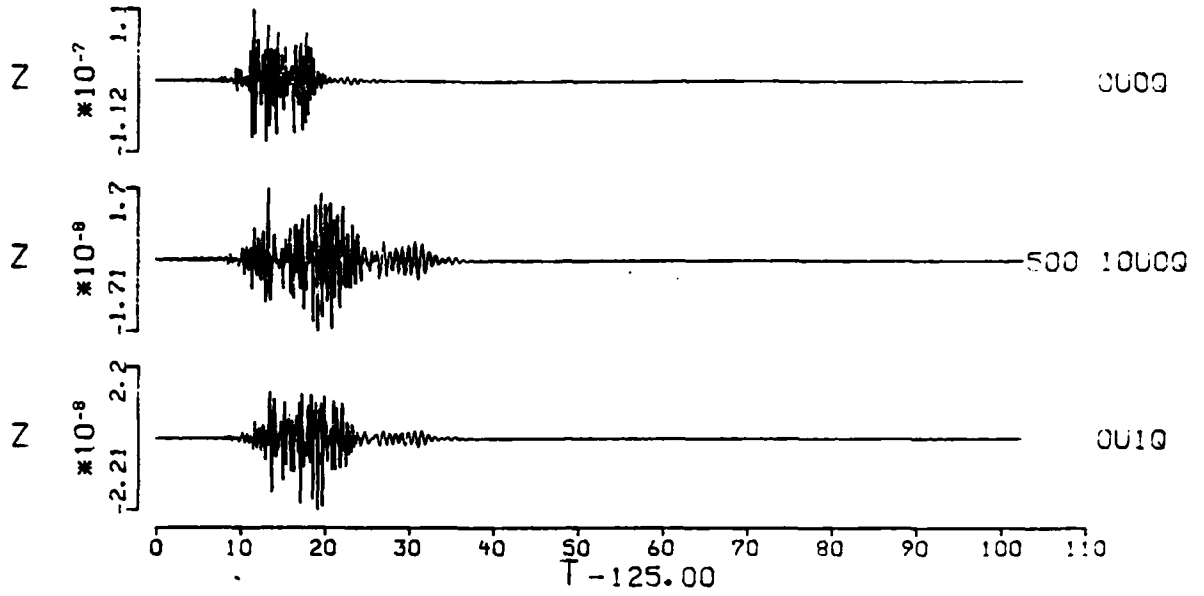

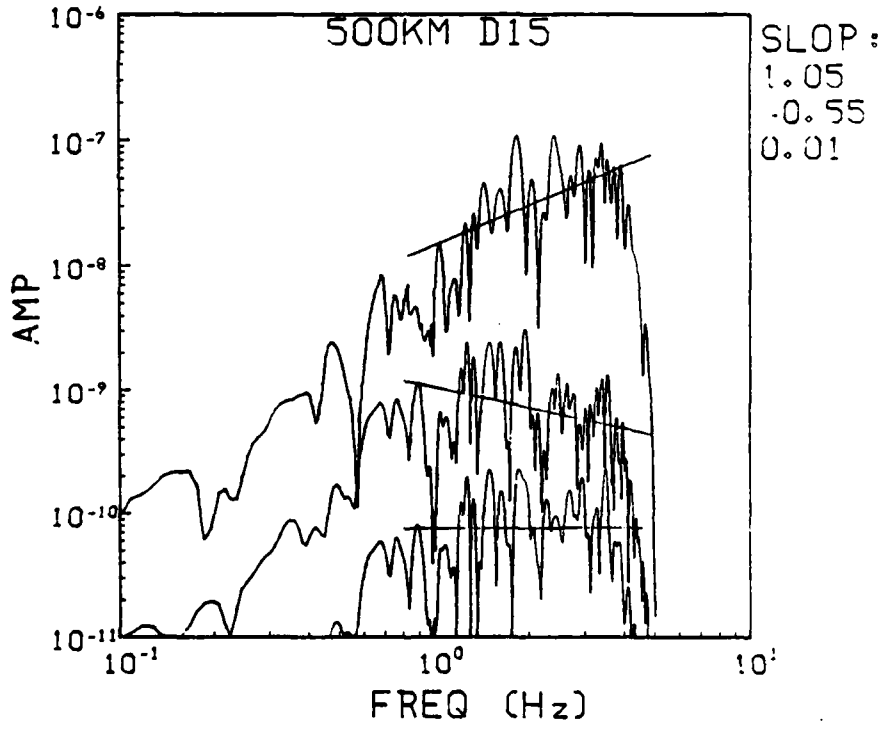

Figure 12b. Same as for Figure 12a, but for scatterer at 15 km deep. Note that the high frequency spectrum slope difference between 0U0Q (undissipative) and 10U0Q (scattering attenuation) cases are very similar for all cases in Figures 11 and 12. The scattering Q is dominant in controlling the frequency decay.

(a)

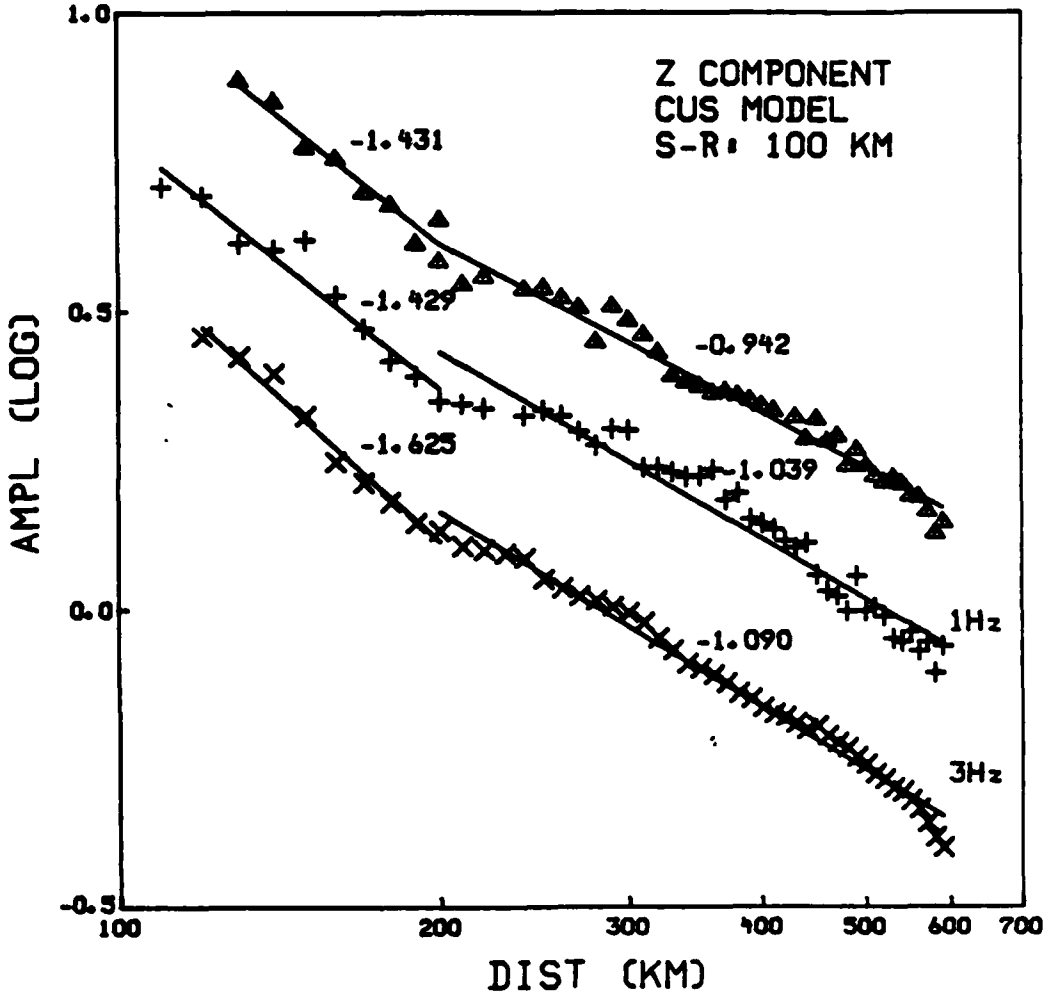

Figures 13. The geometrical spreading factor for scattering waves in the layered medium. Displays are for Z component (a) and SH component (b) with epicentral distance at 100 km in CUS model. The scattering distance varies from 110 km to 600 km. The top curve is from the average peak-to-peak amplitude of composed scattering waveforms, and the lower two curves are for amplitudes after narrow bandpass filtered at 1 Hz and 3 Hz respectively. No Q has been applied. Because of mode conversion, we can see much fast amplitude decay in the front part ($<$200km).

(b)

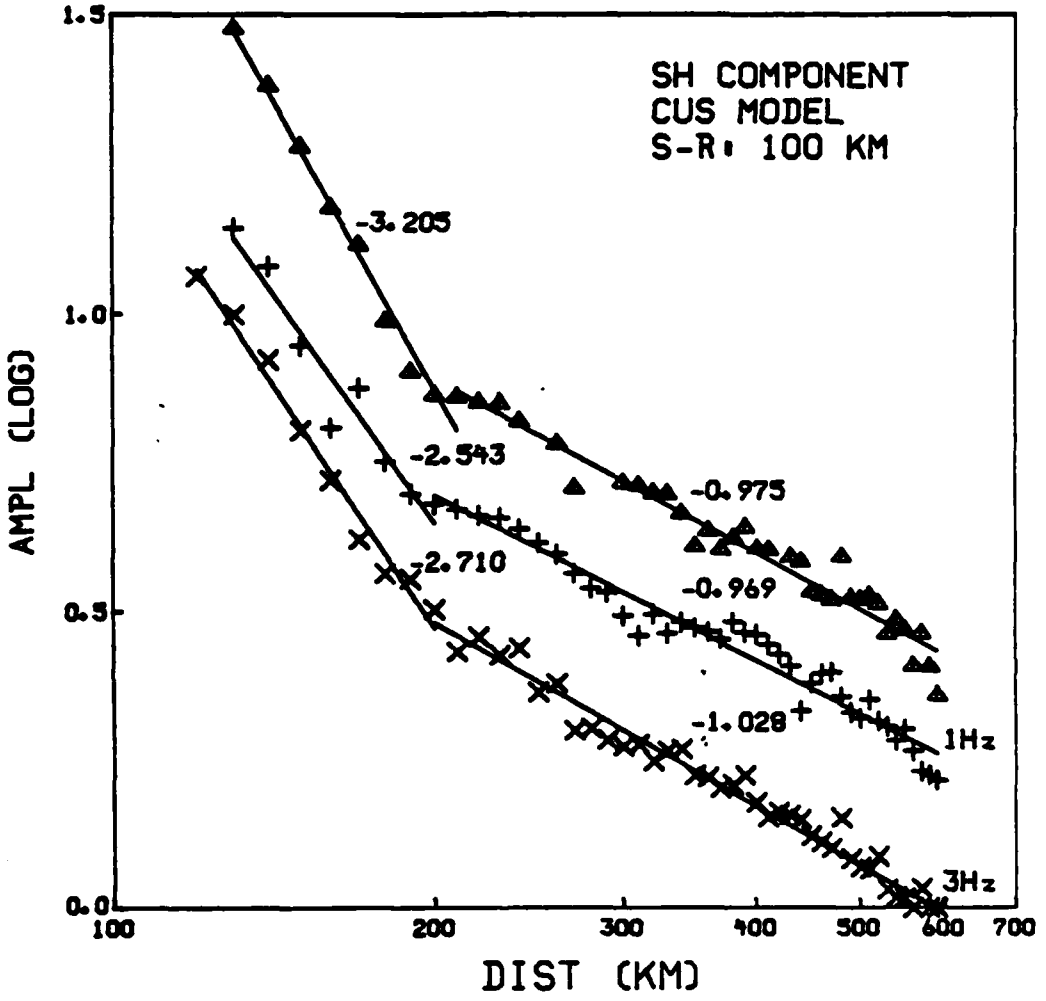
SH COMPONENT
CUS MODEL
S-R= 100 KM
-3.205
-2.543
-2.710
-0.975
-0.969
-1.028
1Hz
3Hz
AMPL (LOG)
DIST (KM)
1.5
1.0
0.5
0.0
100
200
300
400
500
600
700

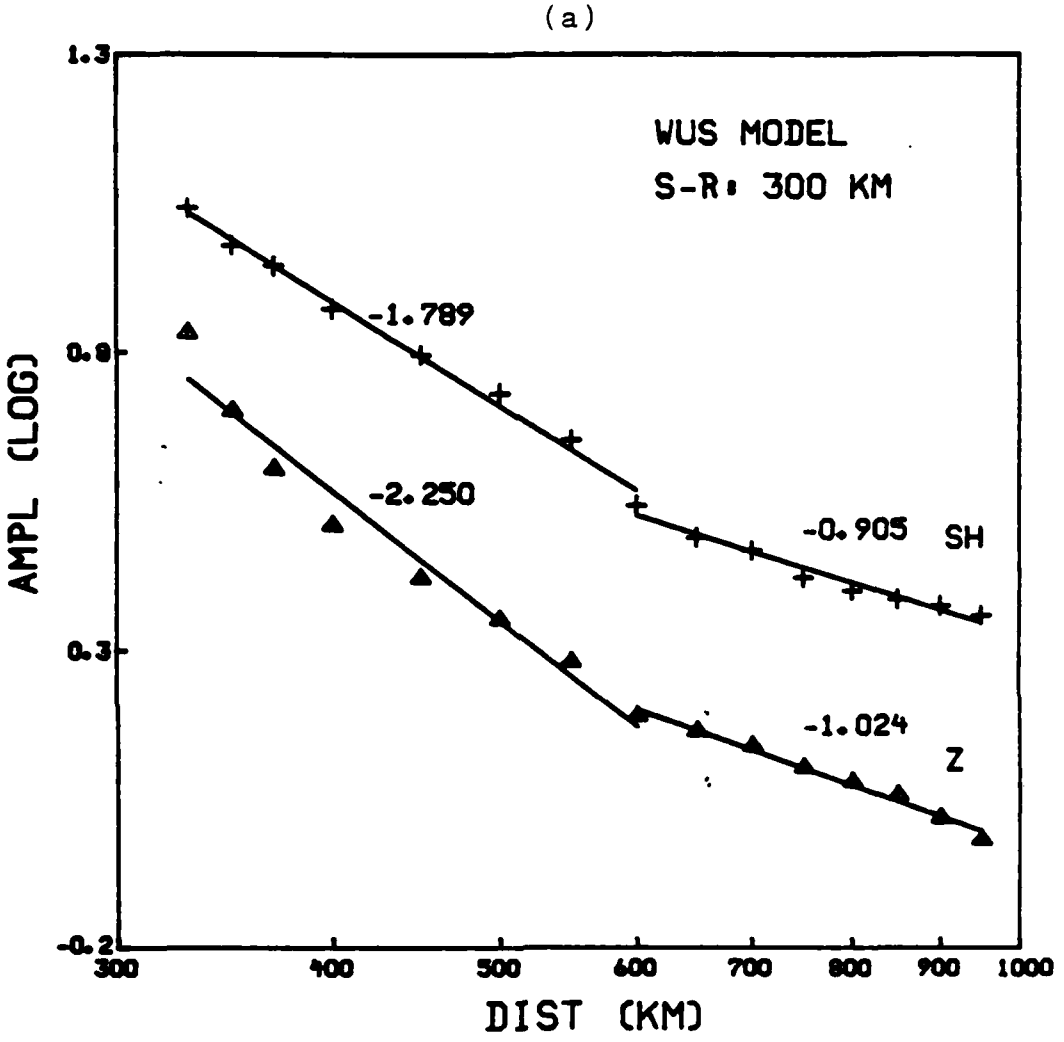

Figure 14. Scattering geometrical spreading in the WUS model. Two components, vertical and tangential, are displayed. (a) is for source -receiver distance at 300 km and (b) at 100 km. Note that the slope changes at 600 km for (a) and at 200 km for (b). The WUS model has more rapid geometrical decay rate than the CUS model. The slope difference between the two regions is also larger.

(b)

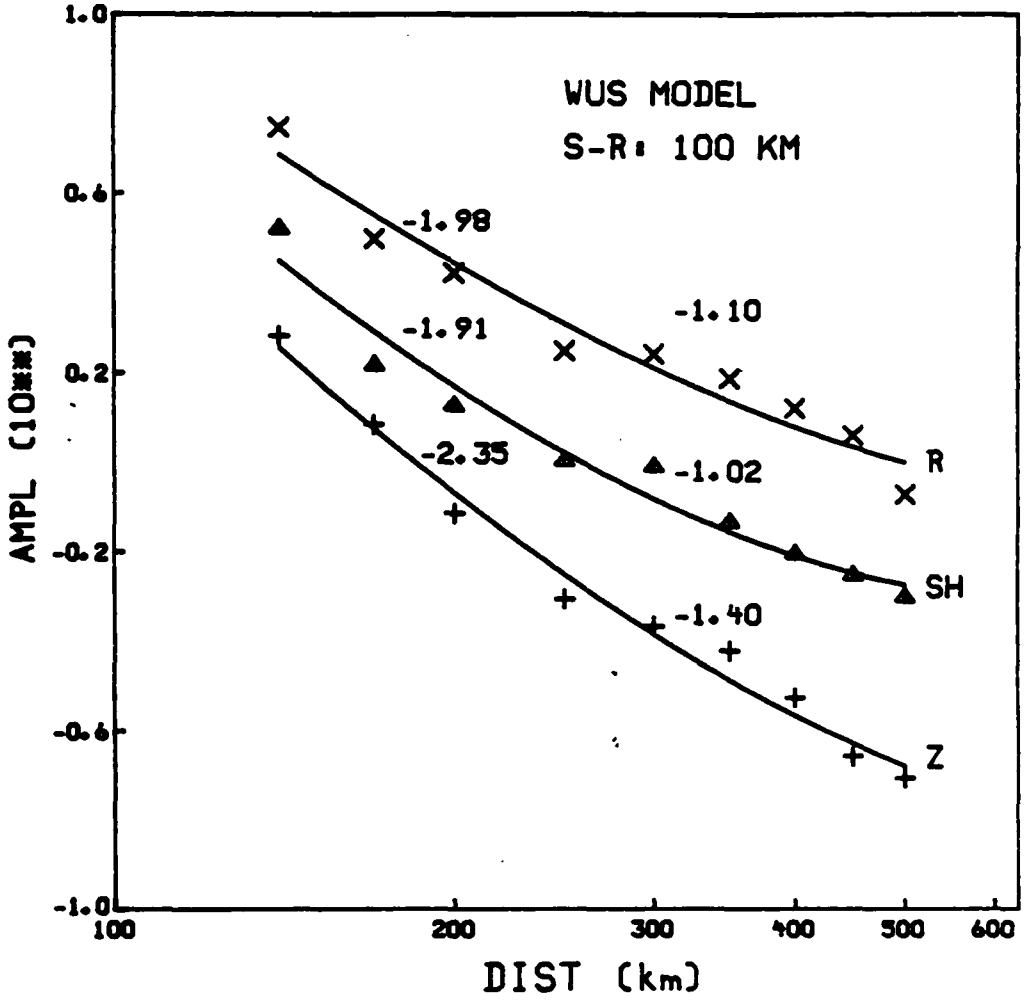
WUS MODEL
S-R: 100 KM
-1.98
-1.10
-1.91
-2.35
-1.02
-1.40
R
SH
Z
AMPL (10**m)
DIST (km)
1.0
0.6
0.2
-0.2
-0.6
-1.0
100
200
300
400
500
600

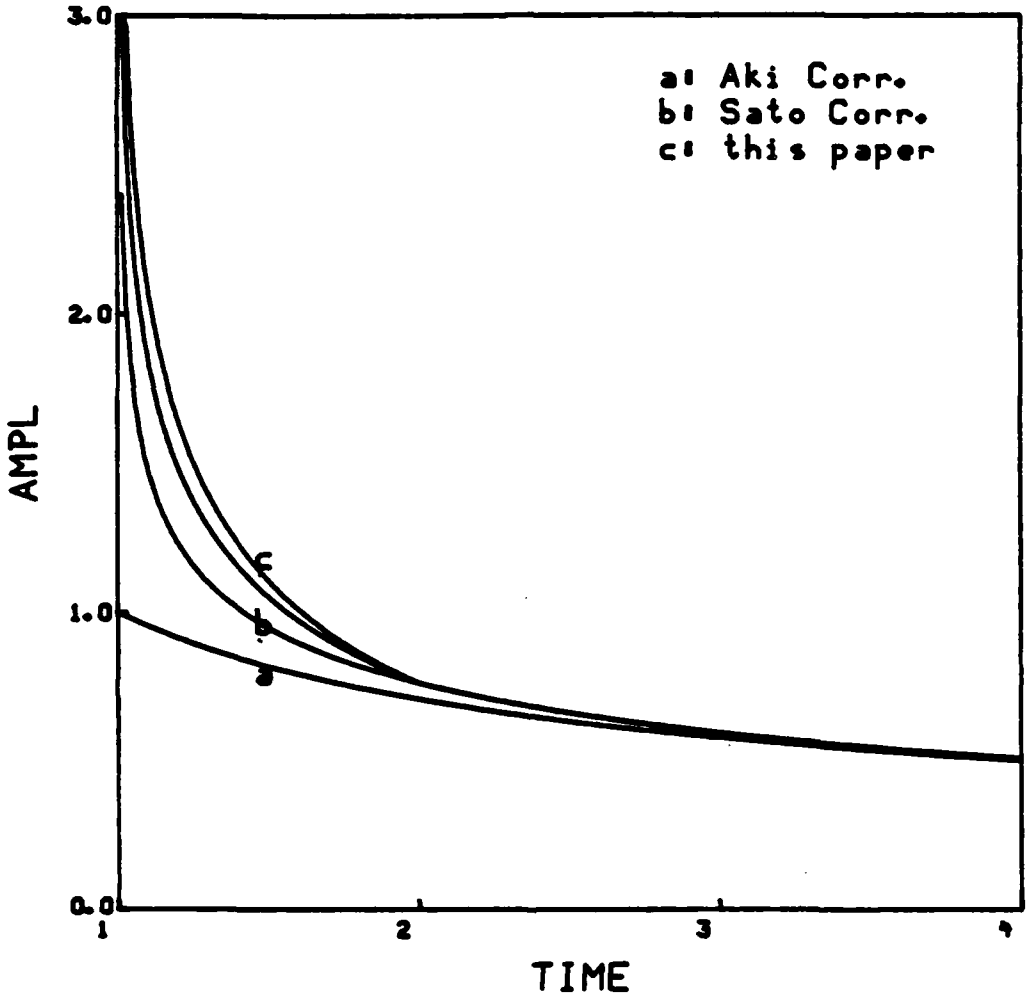

Figure 15. A modification of geometrical spreading correction of Sato's surface-wave scattering model. A higher decay rate of $t^{-0.5}$ to t^{-1} due to mode conversion and wave-type conversion is assumed for the lapse time ratio smaller than 2.

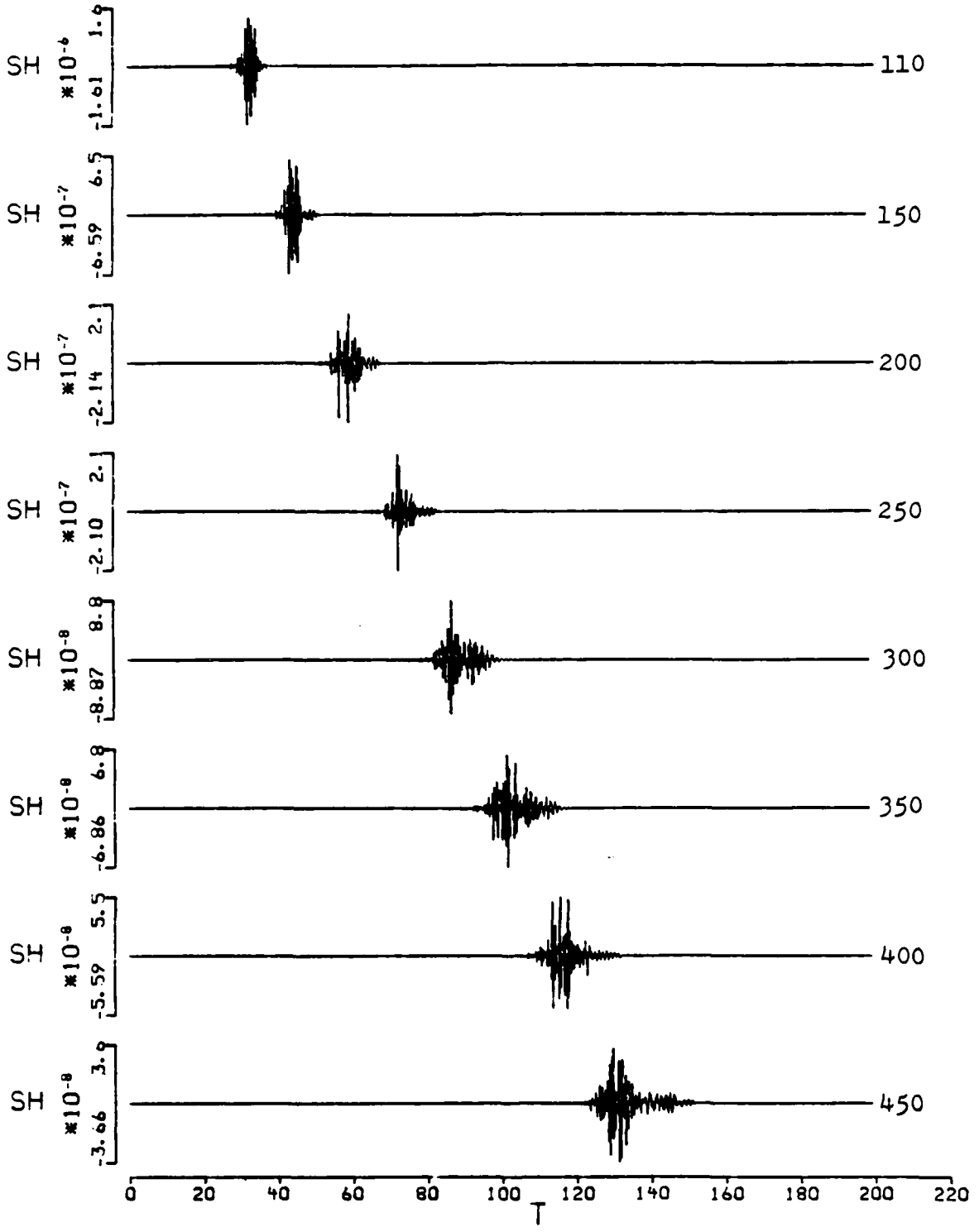

Figure 16a. Scattering pulses at different scattering distances. A Q model 10U1Q has been applied. We use this to measure the pulse duration expansion with traveling distance.

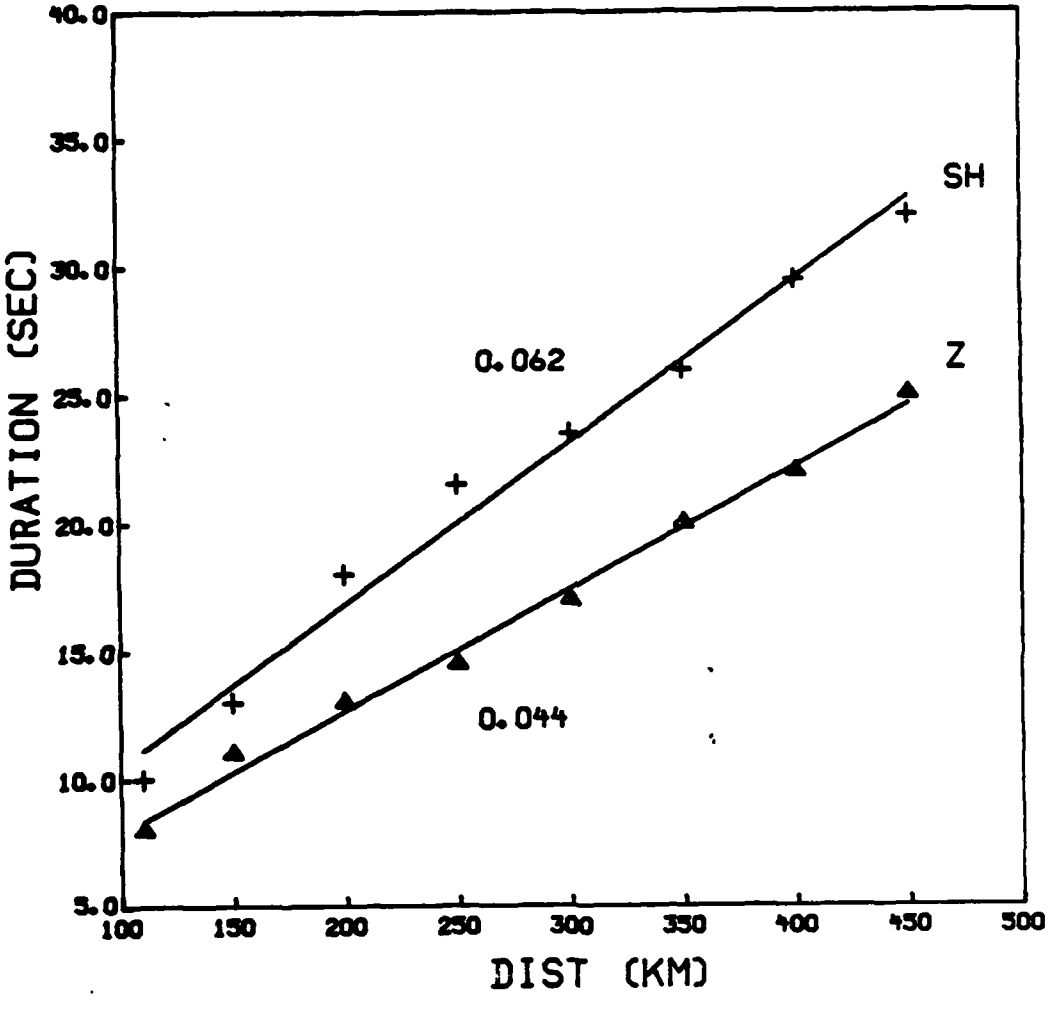

Figure 16b. The duration change measured from Figure 16a are plotted in linear scale with the distance. A duration expansion rate 0.05 with distance is obtained. The upper and lower sets of data are from SH and Z synthetics, respectively.

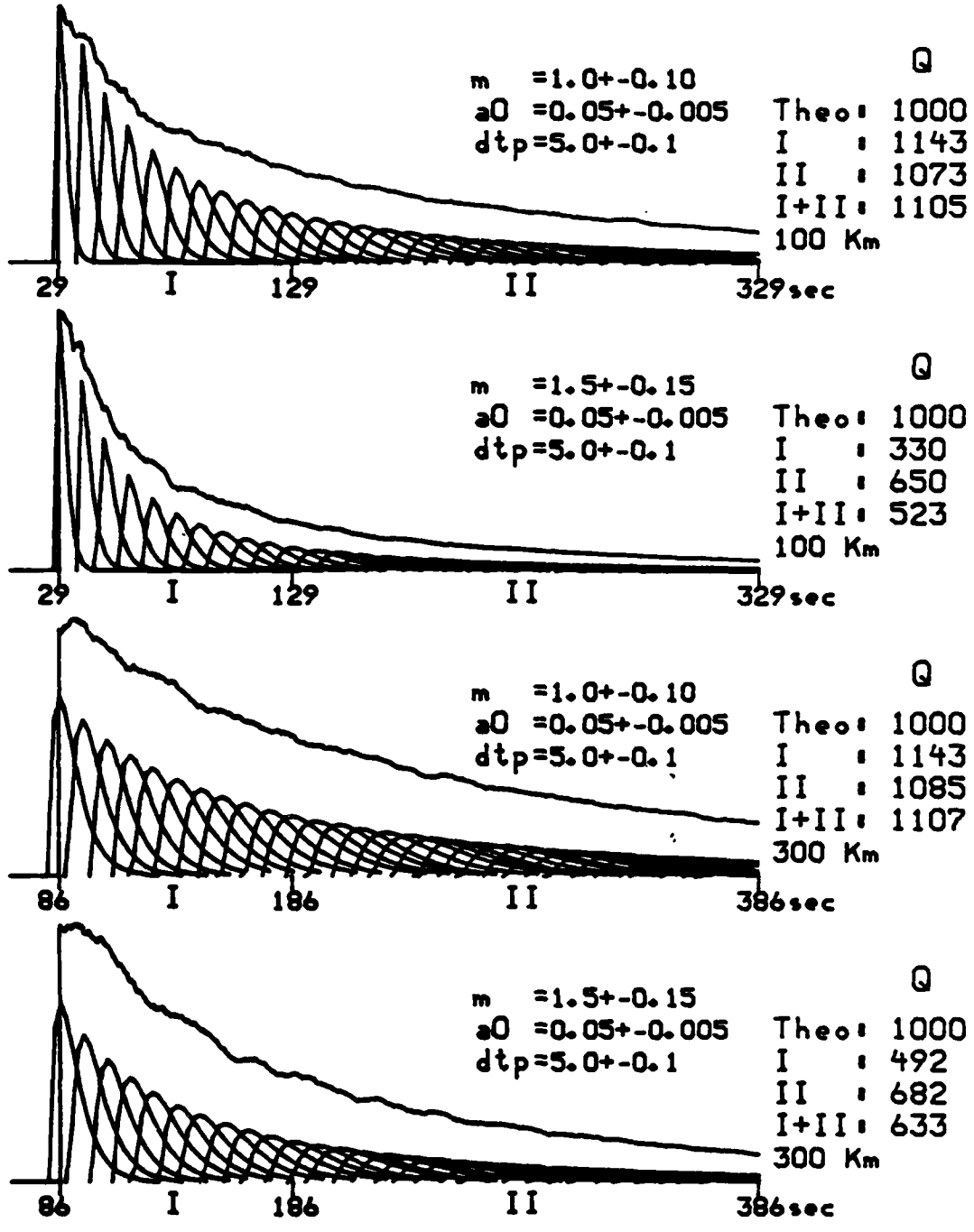

Figure 17a. Superposition of scattering pulses to form the coda envelope. This simulates the eastern United States case. Spreading factor m largely affects the coda decay. Also note that the analysis of first part (I) and the rest (II) yields different apparent Q values.

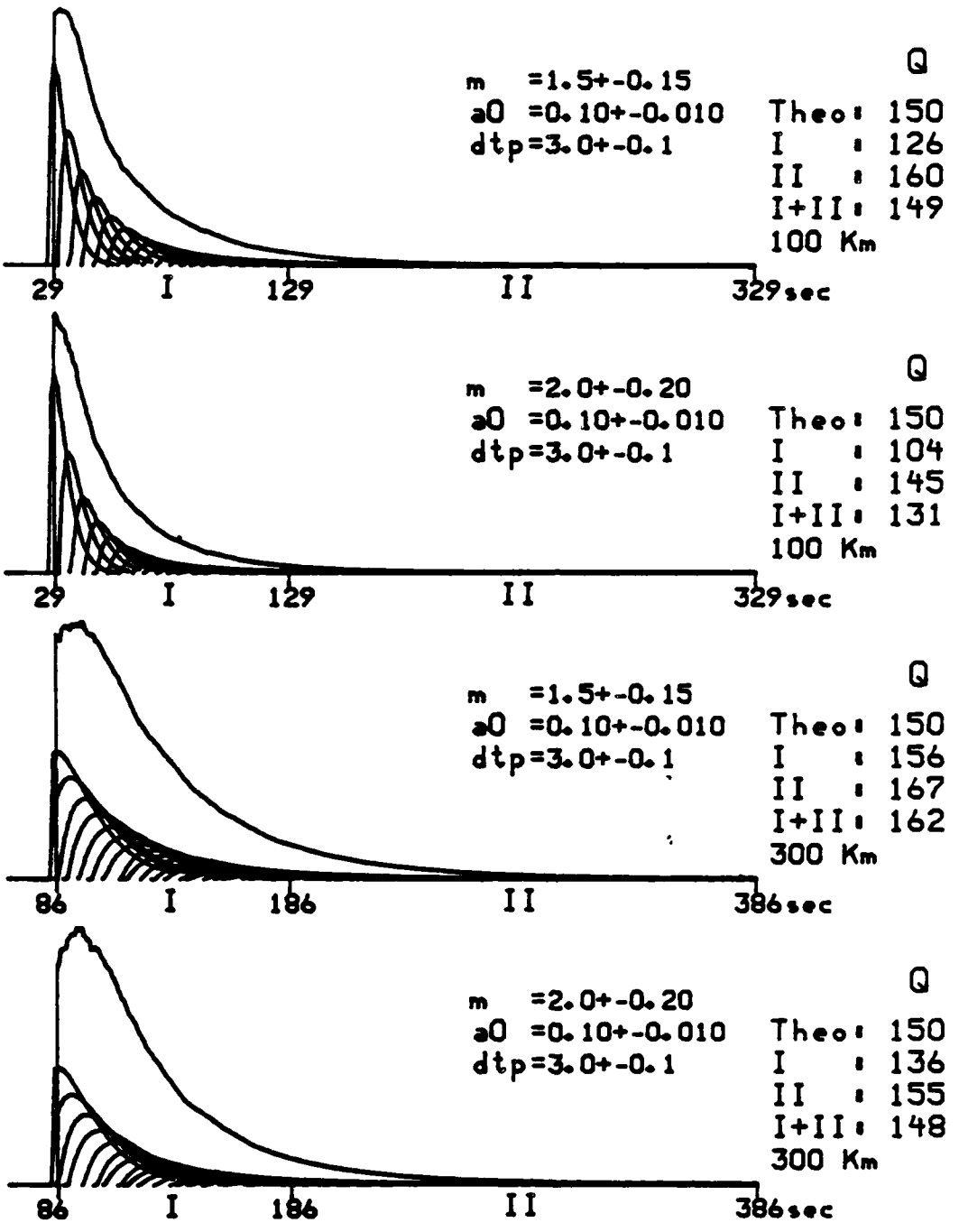

Figure 17b. Same as for Figure 17a. This simulates the western United States case. Since the pulse superposition has been saturated by the rapid decay due to Q, the inferred Q is not dependent upon the shape factors of the individual scattered pulses much.

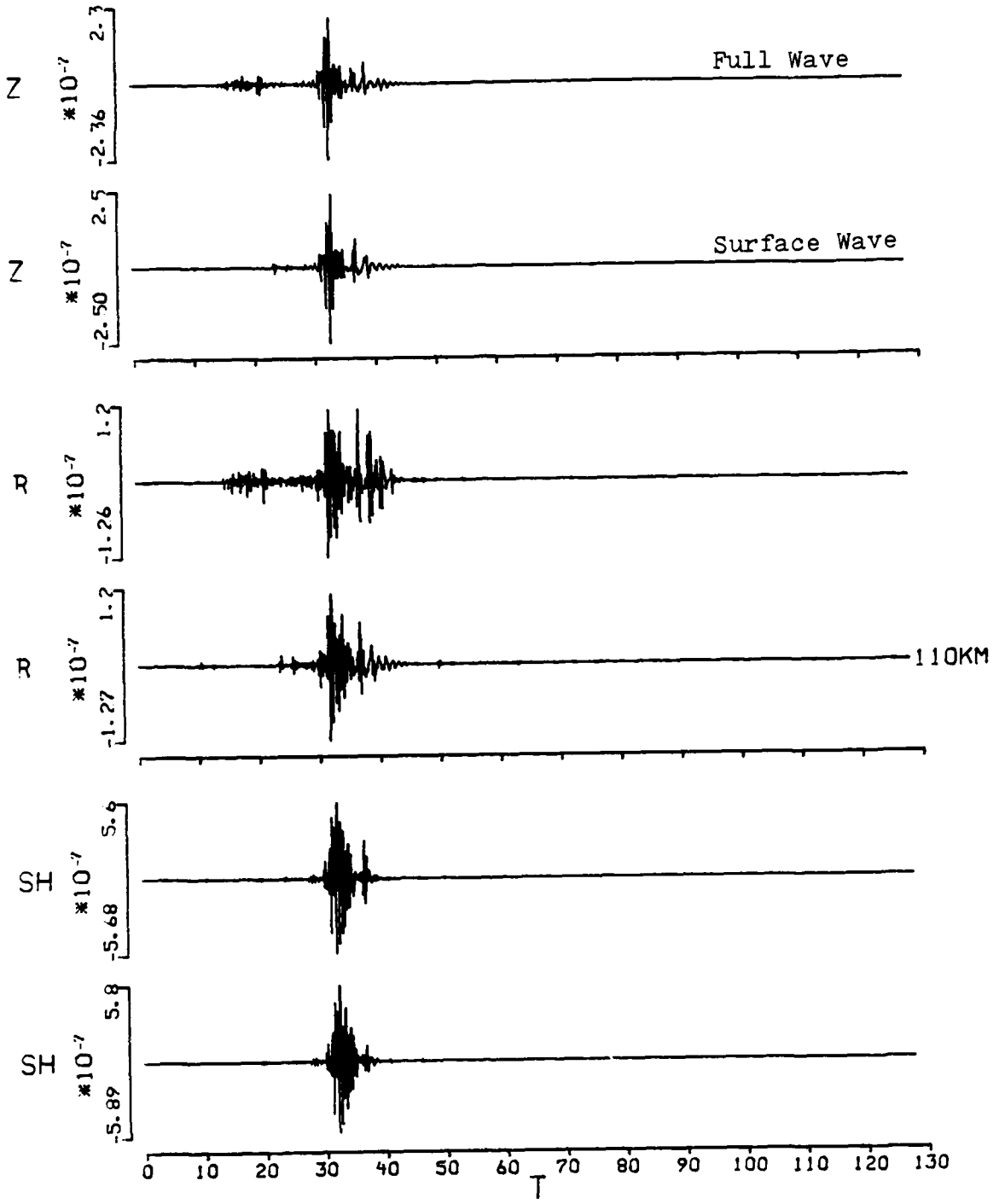

Figure 18. A comparison of body wave and surface wave scattering. The scattering distance is 110 km with epicentral distance at 100 km in the CUS model. Some body and surface wave scattering interaction can be seen.

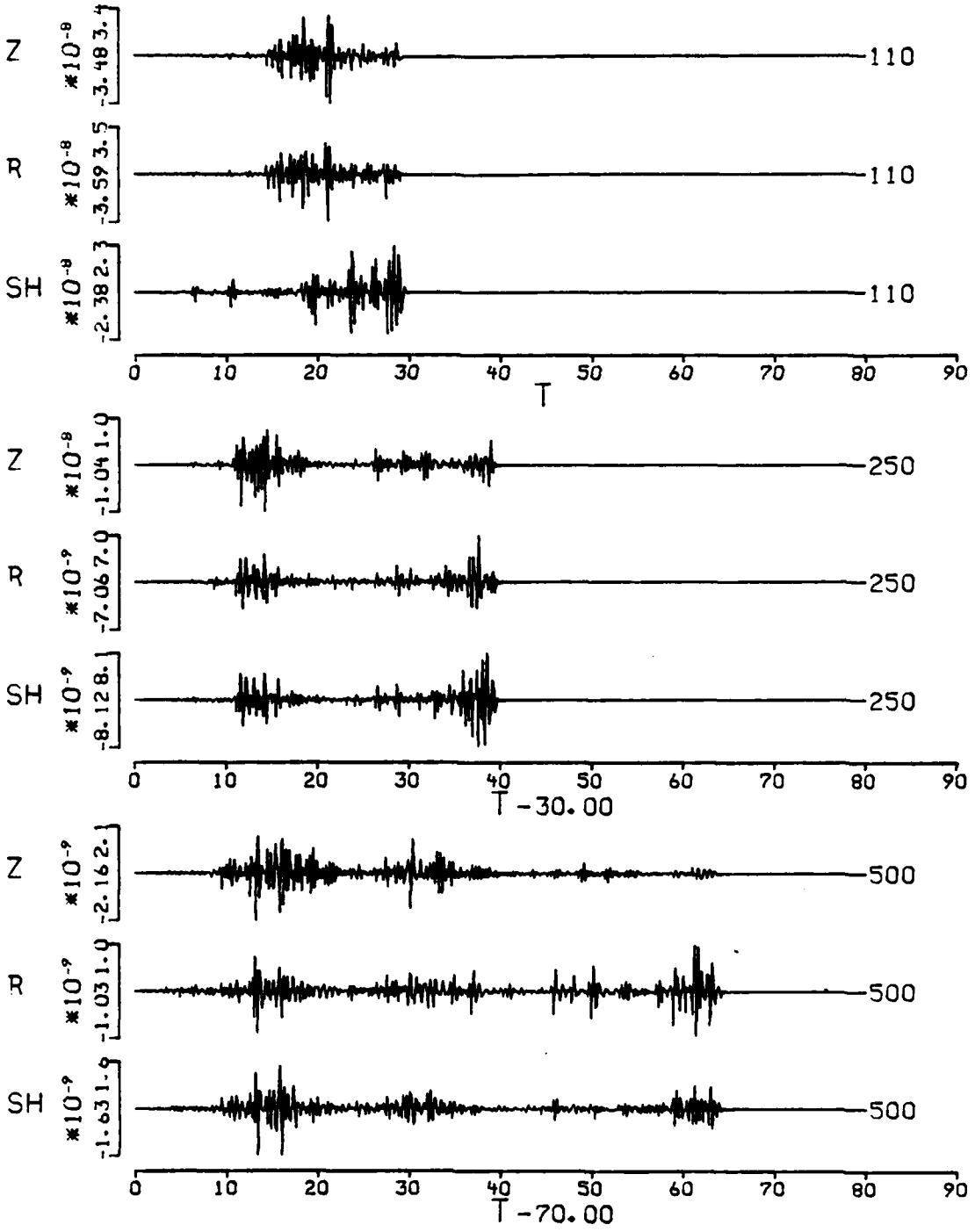

Figure 19. Body-wave scattering expanded at three scattering distances. The scattered waveform is complicated and contains high frequencies. P-wave scattering is strong on the Z component, and S-wave scattering is strong on the two horizontal components. The complicated waveforms show the ray path effect in the layered structure.

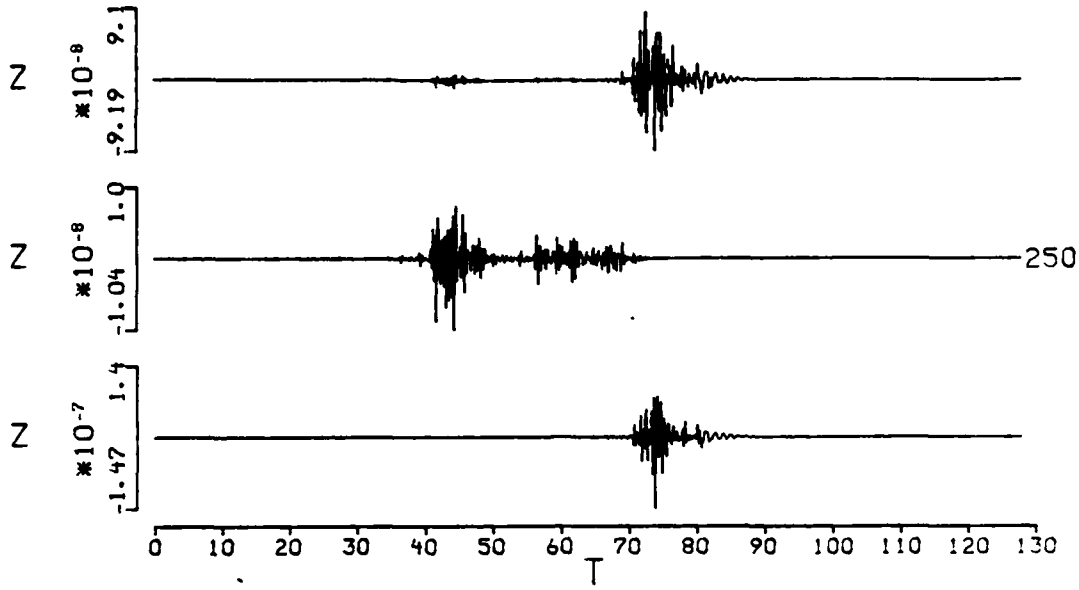

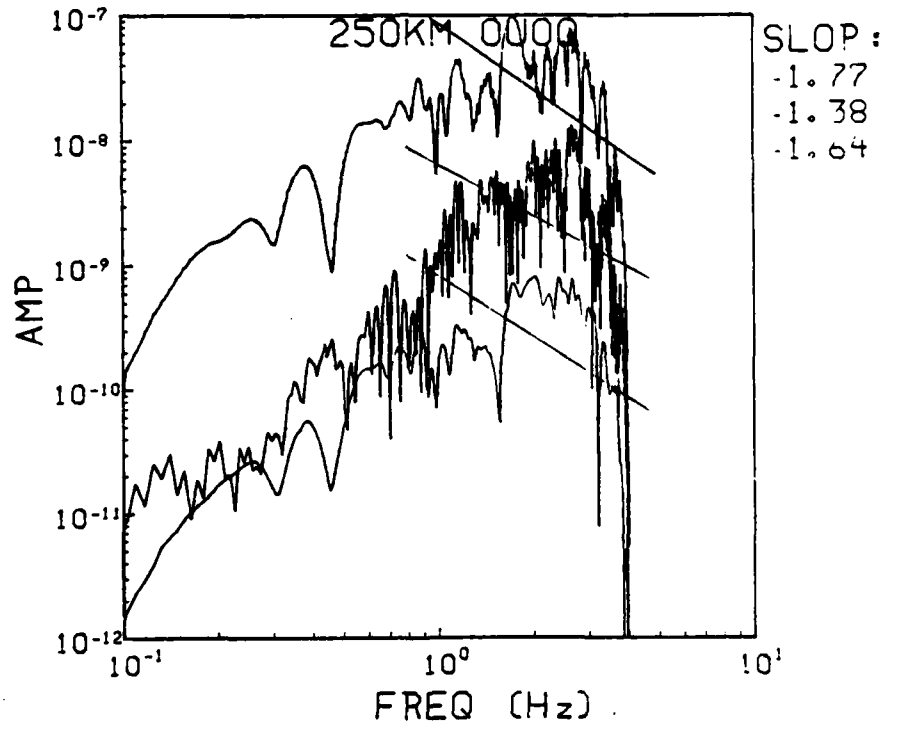

Figure 20a. The spectra of body-wave and surface-wave scattered pulses. Three traces are for complete, body-wave only, and surface-wave only. The spectra of surface-wave only is shifted down by a factor of 100 for clarity. Note that the spectra of the scattered body waves is enriched in high frequencies, even though no attenuation is included.

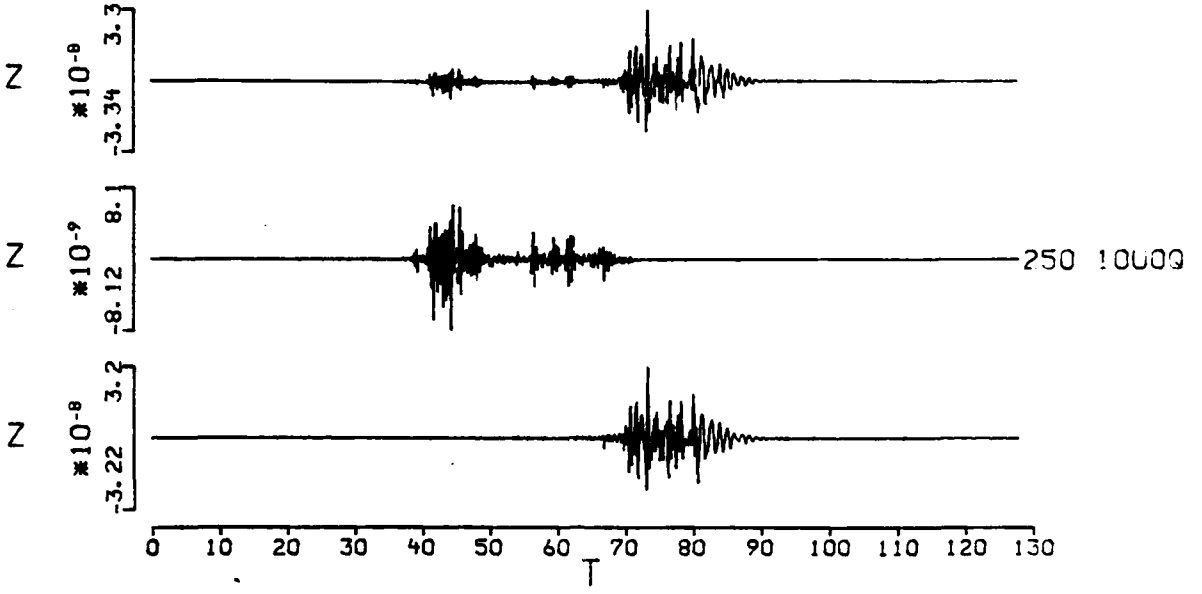

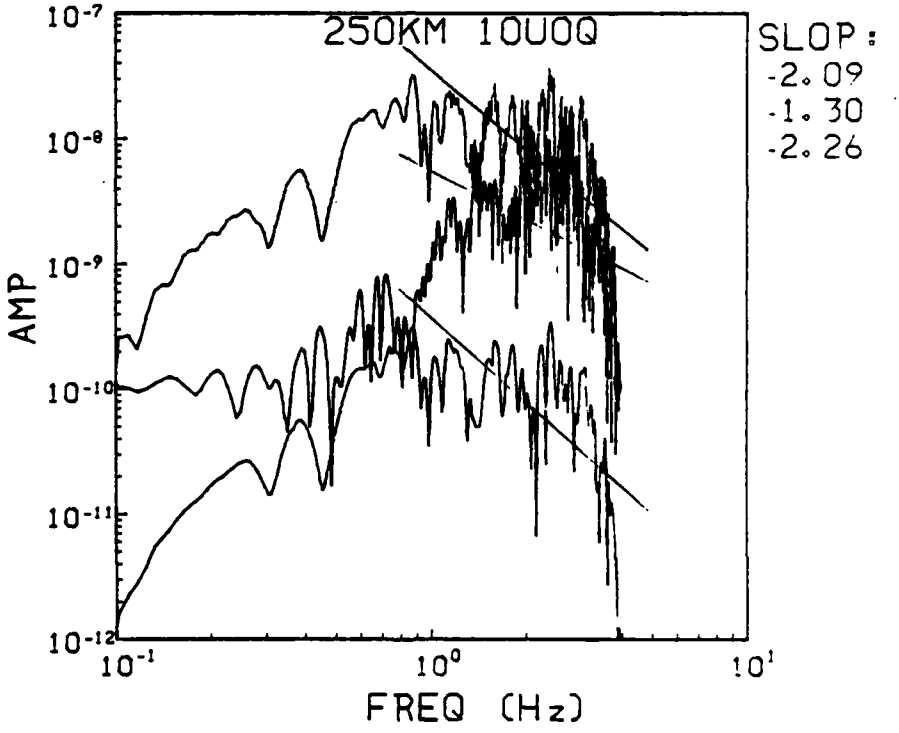

Figure 20b. Same as for Figure 20a with a scattering Q included. The attenuation of body-wave scattered waveforms is less than the surface-wave scattered arrivals.

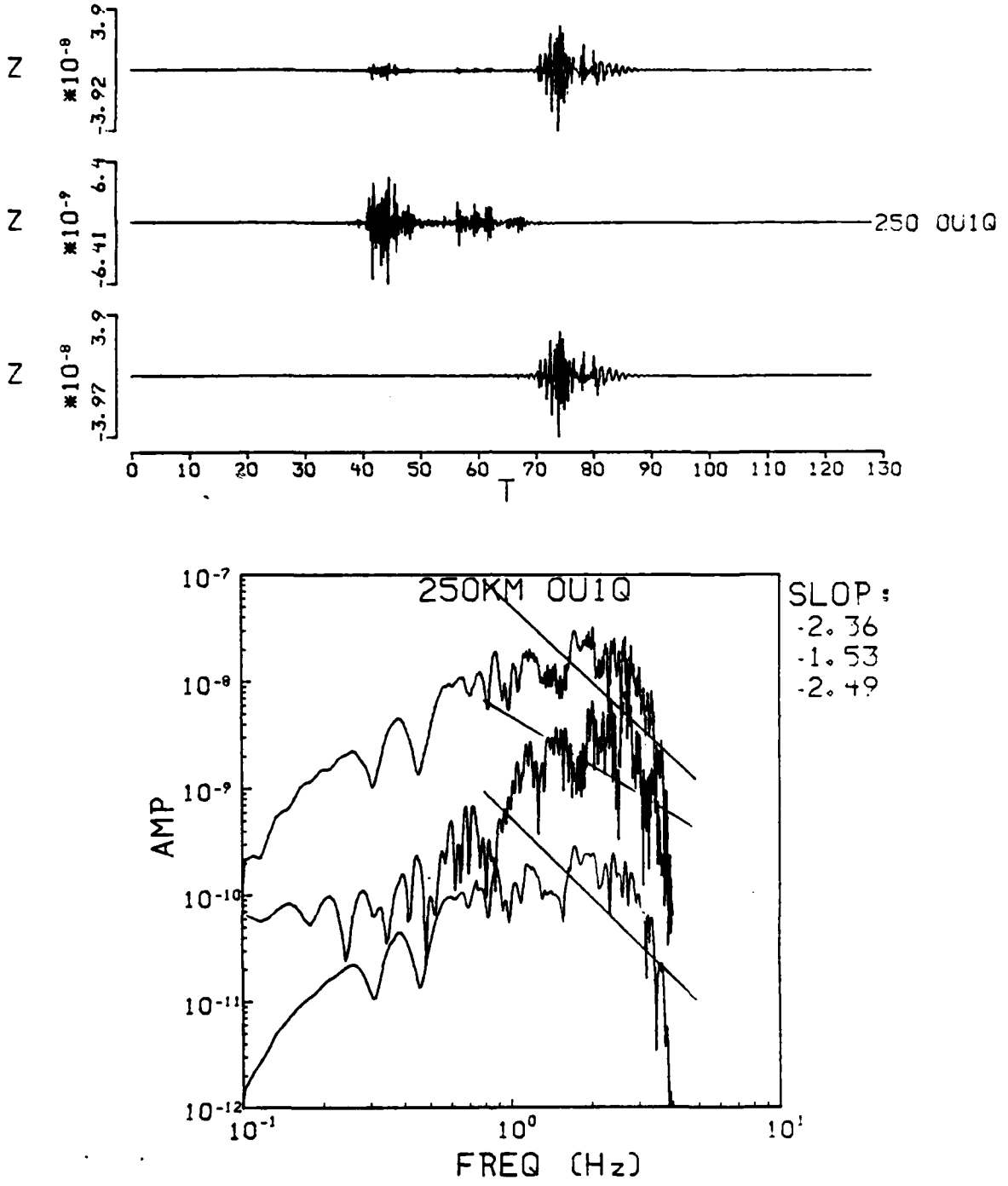

Figure 20c. Same as for Figure 20a with an anelastic Q applied. Again, the body wave scattering shows stronger resistance to attenuation.

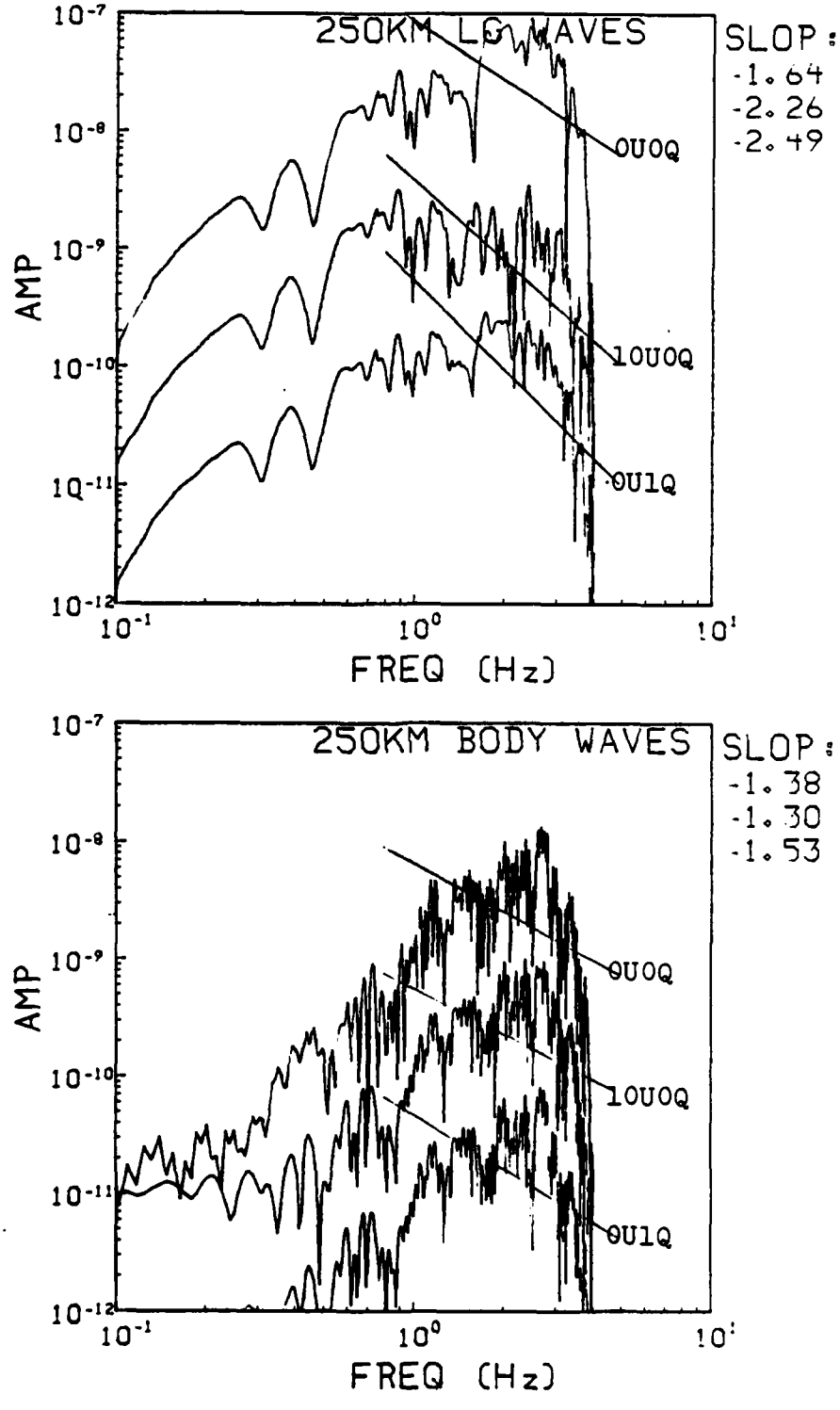

Figure 21a. The decay of high frequency component under different attenuation conditions for surface-wave and body-wave scattering. The body-wave scattering shows much smaller attenuation compared to surface-wave scattering attenuation. Each spectrum has been shifted by a factor of ten for clarity.

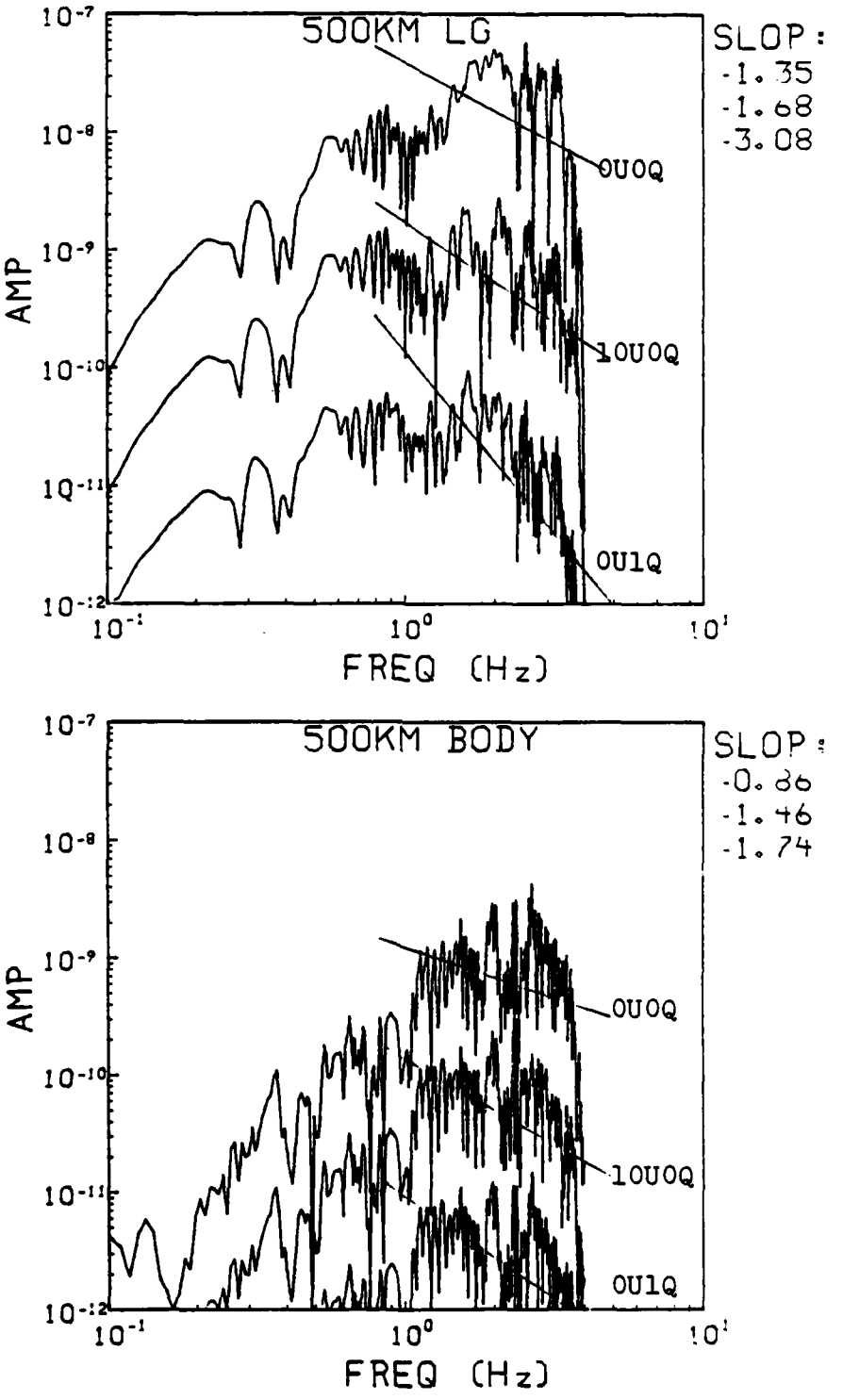

Figure 21b. same as for Figure 21a, but for a scattering distance of 500 km. The frequency content of body-wave scattering seems not affected as much by the attenuation.

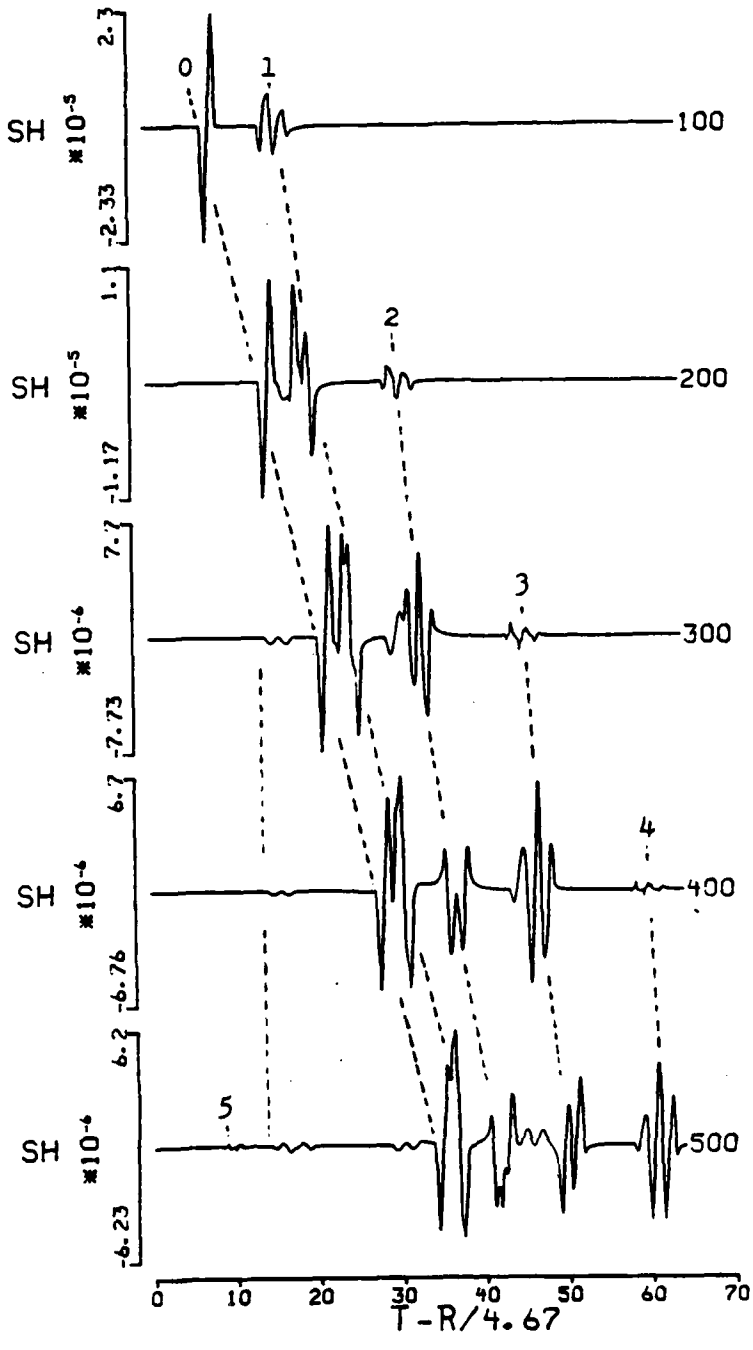

Figure 22. The synthetic seismograms from 'locked mode' approximation. SH component from a single layer over halfspace model (SCM) is plotted with different epicentral distance. The arrivals from different reverberation are followed through the section.

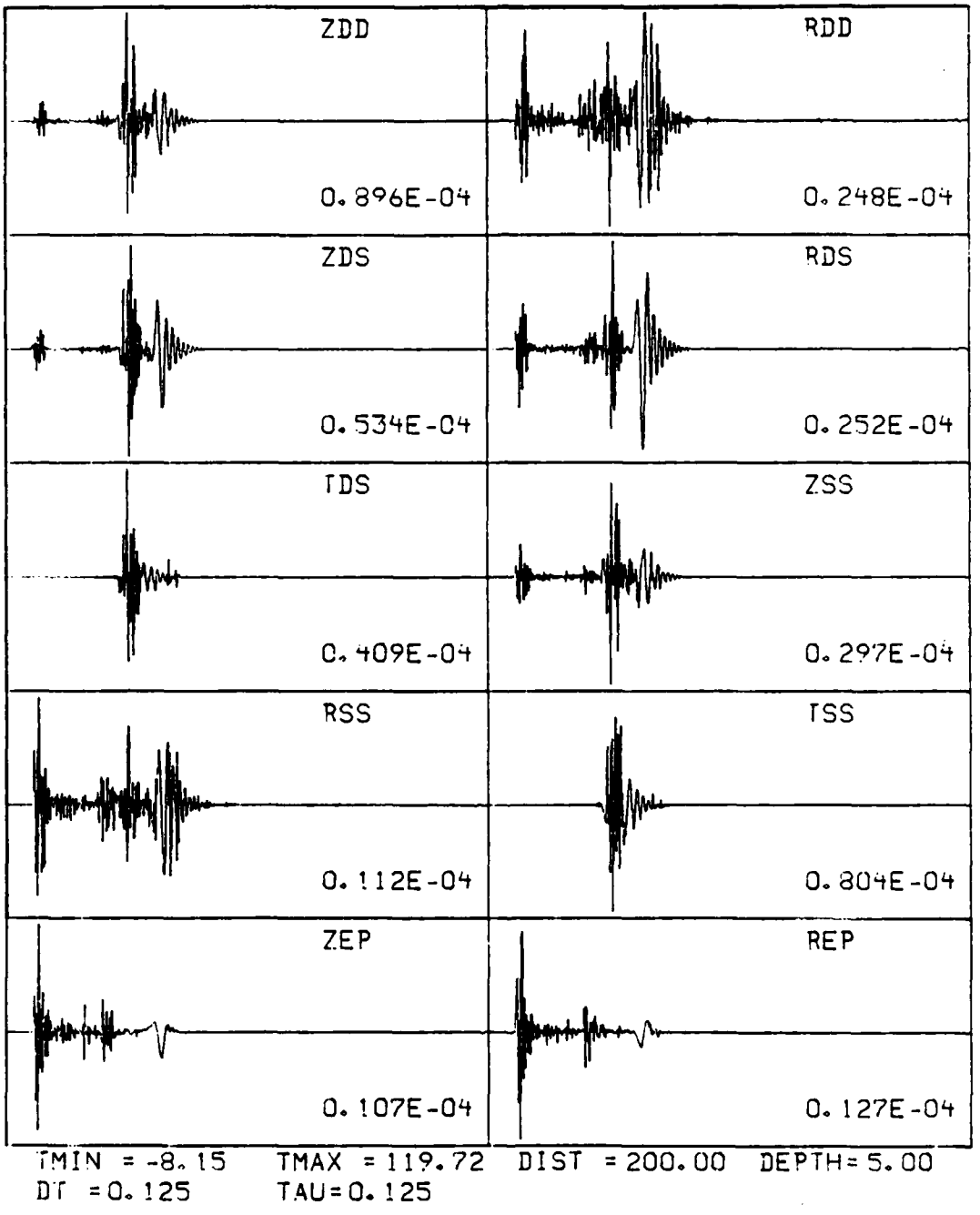

Figure 23. Ten basic type complete seismograms generated by locked mode approximation method. The seismograms rather have excellent quality.